Chemical Geology 265 (2009) 321–334

Contents lists available at ScienceDirect

Chemical Geology

journal homepage: www.elsevier.com/locate/chemgeo

Aqueous geochemistry and oxygen isotope compositions of acid mine drainage from the Río Tinto, SW Spain, highlight inconsistencies in current models

Christopher G. Hubbard [a,b,*], Stuart Black [a], Max L. Coleman [a,b]

[a] School of Human and Environmental Science, University of Reading, The University of Reading, Whiteknights, PO Box 227, Reading RG6 6AB, UK
[b] NASA Astrobiology Institute and Jet Propulsion Laboratory, California Institute of Technology, M/S 183-301, 4800 Oak Grove Drive, Pasadena, CA 91109, USA

ARTICLE INFO

Article history:
Received 28 August 2008
Received in revised form 4 April 2009
Accepted 11 April 2009

Editor: D. Rickard

Keywords:
Oxygen isotopes
Acid mine drainage
Pyrite oxidation
Río Tinto

ABSTRACT

The Río Tinto river in SW Spain is a classic example of acid mine drainage and the focus of an increasing amount of research including environmental geochemistry, extremophile microbiology and Mars-analogue studies. Its 5000-year mining legacy has resulted in a wide range of point inputs including spoil heaps and tunnels draining underground workings. The variety of inputs and importance of the river as a research site make it an ideal location for investigating sulphide oxidation mechanisms at the field scale. Mass balance calculations showed that pyrite oxidation accounts for over 93% of the dissolved sulphate derived from sulphide oxidation in the Río Tinto point inputs. Oxygen isotopes in water and sulphate were analysed from a variety of drainage sources and displayed $\delta^{18}O_{(SO4-H2O)}$ values from 3.9 to 13.6‰, indicating that different oxidation pathways occurred at different sites within the catchment. The most commonly used approach to interpreting field oxygen isotope data applies water and oxygen fractionation factors derived from laboratory experiments. We demonstrate that this approach cannot explain high $\delta^{18}O_{(SO4-H2O)}$ values in a manner that is consistent with recent models of pyrite and sulphoxyanion oxidation. In the Río Tinto, high $\delta^{18}O_{(SO4-H2O)}$ values (11.2–13.6‰) occur in concentrated (Fe = 172–829 mM), low pH (0.88–1.4), ferrous iron (68–91% of total Fe) waters and are most simply explained by a mechanism involving a dissolved sulphite intermediate, sulphite–water oxygen equilibrium exchange and finally sulphite oxidation to sulphate with O_2. In contrast, drainage from large waste blocks of acid volcanic tuff with pyritiferous veins also had low pH (1.7), but had a low $\delta^{18}O_{(SO4-H2O)}$ value of 4.0‰ and high concentrations of ferric iron (Fe(III) = 185 mM, total Fe = 186 mM), suggesting a pathway where ferric iron is the primary oxidant, water is the primary source of oxygen in the sulphate and where sulphate is released directly from the pyrite surface. However, problems remain with the sulphite–water oxygen exchange model and recommendations are therefore made for future experiments to refine our understanding of oxygen isotopes in pyrite oxidation.

1. Introduction

The Río Tinto in SW Spain flows for some 100 km from its origin in the Iberian Pyrite Belt to its common estuary with the adjacent Río Odiel, by the city of Huelva. Acid mine drainage emanates from a wide range of sources (gangue materials from ore extraction, smelting residues, settling ponds, waste from heap leaching and tunnels draining underground workings) in the disused Peña del Hierro and Río Tinto mines located in the river's headwaters (Fig. 1). The range of sources makes this field site an excellent natural laboratory for investigating variations in sulphide oxidation mechanisms.

Acid mine drainage is predominantly caused by the oxidation of pyrite (FeS_2), the most common sulphide mineral found in base metal and coal deposits. Pyrite oxidation is often represented by Eqs. (1)–(3), with either atmospheric oxygen or ferric iron as the oxidant.

$$FeS_2 + 3.5O_2 + H_2O \rightarrow Fe^{2+} + 2SO_4^{2-} + 2\,H^+ \quad (1)$$

$$Fe^{2+} + H^+ + 0.25O_2 \rightarrow Fe^{3+} + 0.5H_2O \quad (2)$$

$$FeS_2 + 14Fe^{3+} + 8H_2O \rightarrow 15Fe^{2+} + 2SO_4^{2-} + 16\,H^+ \quad (3)$$

Oxidation by Fe^{3+} has been shown to oxidize pyrite 18 to 170 times more rapidly than O_2 (Nordstrom and Alpers, 1999). However, this step is limited by the rate of ferrous iron oxidation (Eq. (2)), which is greatly increased (by up to 5 orders of magnitude; Nordstrom and Alpers, 1999) through the action of Fe-oxidizing chemolithoautotrophs, such as the bacteria *Acidithiobacillus ferrooxidans* and *Leptospirillum ferrooxidans*. Although Eqs. (1)–(3) may represent the stoichiometry of pyrite oxidation, they do not give sufficient information about the underlying mechanisms. Each S atom loses 7 electrons yet electron transfer

* Corresponding author. School of Earth and Environment, University of Leeds, Leeds LS2 9JT, UK.
E-mail addresses: chris.hubbard@fastmail.fm, c.g.hubbard@leeds.ac.uk (C.G. Hubbard).

0009-2541/$ – see front matter © 2009 Elsevier B.V. All rights reserved.
doi:10.1016/j.chemgeo.2009.04.009

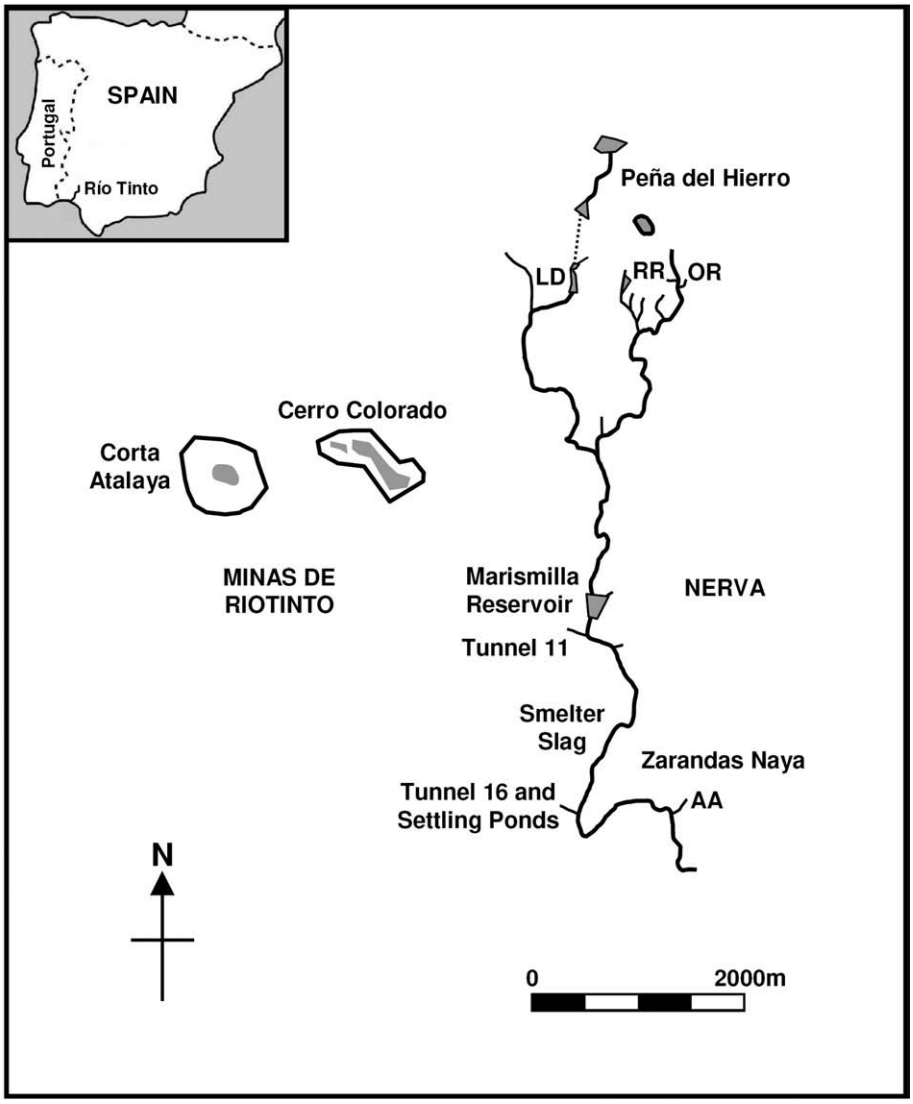

Fig. 1. Location map showing the headwaters of the Río Tinto. Town names in capitals. AA = Arroyo Alcojola, LD = Lake Doughnut, OR = Ochre River, RR = Red River.

reactions generally involve only one or two electrons (Basolo and Pearson, 1967), implying that there are a number of intermediate steps between S^{-} and SO_4^{2-}. However, there is still considerable debate as to what these steps are, where they occur (on the pyrite surface or in the surrounding water) and how they are influenced by biological and physicochemical factors such as pH, Eh, dissolved O_2 concentrations, Fe^{3+} concentrations, temperature, isotopic exchange with water and microbial ecology (Schippers et al., 1996; Borda et al., 2003b; Druschel et al., 2003a,b; Nordstrom et al., 2007).

One method with the potential to further constrain oxidation mechanisms is the use of sulphate–oxygen isotopes. Two main sources of sulphate–oxygen have been proposed: water ($\delta^{18}O$ generally <0‰) and atmospheric oxygen ($\delta^{18}O = 23.5 \pm 0.3$‰; Kroopnick and Craig, 1972). If $\delta^{18}O_{SO4}$ and $\delta^{18}O_{H2O}$ are measured and the fractionation factors involved in the incorporation of water–oxygen (ε_{H2O}) and atmospheric oxygen (ε_{O2}) into sulphate are known, then the sources of sulphate–oxygen can be determined (Taylor et al., 1984a,b; van Everingden and Krouse, 1985; Taylor and Wheeler, 1994). The possibility of isotopic exchange between water and any dissolved sulphoxyanions also needs to be considered. Isotopic exchange with sulphate is slow (360 years at pH 1.0 and 25 °C, estimated from Fig. 8 in Seal (2003) based on data from Chiba and Saki (1985) and Hoering and Kennedy (1957)) but dissolved sulphite exchanges oxygen with water at a much faster rate (half-life, $t(1/2) = 25.3$ h at pH 10.5 and 1.3 min at pH 8.9, Betts and Voss (1970)). No data are available for sulphite-water oxygen exchange kinetics at lower pH, where bisulphite rather than sulphite dominates. A log–linear relationship between pH and oxygen exchange rates may hold true for the sulphite/bisulphite system as it does for the sulphate/bisulphate system (Fig. 8 in Seal (2003)) but this has not yet been confirmed.

The fraction of water–oxygen incorporated into sulphate during pyrite oxidation can be determined explicitly from controlled oxidation experiments with a range of initial $\delta^{18}O_{H2O}$. The gradient of a plot of $\delta^{18}O_{SO4}$ and $\delta^{18}O_{H2O}$ gives the proportion of water–oxygen incorporated into sulphate (Gould et al., 1989; Balci et al., 2007). No such constraint is possible for the interpretation of field data, which relies on models derived from laboratory experiments. However field data are essential to validate the proposed models by applying them to environmental conditions outside of the experiments from which they were derived.

An examination of recent literature shows that sulphate–oxygen isotope data are being routinely integrated into field studies of sites affected by pyrite oxidation, including pit lakes (Knoller et al., 2004; Pellicori et al., 2005; Migaszewski et al., 2008), drainage from underground workings (Butler, 2007), mine tailings and waste rocks (Sracek et al., 2004; Seal et al., 2008; Smuda et al., 2008) and as a tracer of contamination in surface/groundwater (Bottrell, 2007; Cortecci et al., 2008). A compilation of earlier field data can be found in Seal (2003).

Pyrite oxidation mechanisms are commonly interpreted using simple fractionation factors and related to oxidation by O_2 (Eq. (1)) or Fe^{3+} (Eq. (3)). Fewer field studies have interpreted the data based on the role of dissolved sulphoxyanion intermediates, specifically sulphite (Seal, 2003; Pellicori et al., 2005; Seal et al., 2008). Interpretation of field data can be further complicated by the fact that processes other than sulphide oxidation can alter $\delta^{18}O_{H2O}$ and/or $\delta^{18}O_{SO4}$. Examples of these include evaporation (e.g. the Penn mine, California; Hamlin and Alpers, 1995, 1996; Seal, 2003), the dissolution of soluble sulphate minerals (e.g. the Animas River in Colorado; Nordstrom et al., 2007), the mixing of different waters (e.g. Freiberg, Germany; Haubrich and Tichomirowa, 2002; Seal, 2003), sulphate reduction subsequent to pyrite oxidation (e.g. the Fontana and Hazel Creek mines, North Colorado; Seal et al., 1998) and sulphate-water oxygen exchange at extreme low pH (e.g. Iron Mountain; Taylor and Wheeler, 1994).

The purpose of this paper is to apply current models of sulphide oxidation and sulphate–oxygen isotope compositions to acid mine drainage from the Río Tinto. Variations in the sources of dissolved sulphate are examined using a mass balance approach. The sulphate–oxygen isotope models are used to identify pyrite oxidation processes in two contrasting oxidation environments and are applied to samples draining underground, inaccessible environments. We also use the Río Tinto field data to highlight and identify inconsistencies in the current models and suggest future laboratory work that may help to constrain models further and increase their use in interpreting field data.

2. Study area

The Río Tinto deposit may originally have formed a single ore body (5 km × 750 m × 40 m) containing over 500 Mt of sulphides (Nehlig et al., 1998). As a result of Hercynian deformation, sulphide mineralisation is now present as a number of ore bodies hosted by shale and acid volcanics and located on the eastern hinge and both limbs of a local anticline that sits within a larger syncline (Nehlig et al., 1998; Tornos, 2006). The Peña del Hierro ore body lies on the northern side of the syncline and is hosted by acid volcanic tuffs. The ore bodies contain pyrite (FeS_2) with minor chalcopyrite ($CuFeS_2$), arsenopyrite (FeAsS), sphalerite (ZnS), galena (PbS) and barite ($BaSO_4$) and were covered by a weathering layer of gossan. Mining activities have been carried out intermittently for some 5000 years (Avery, 1974; Salkield, 1987; van Geen et al., 1997; Ruiz et al., 1998; Leblanc et al., 2000), driven in the past few centuries by the demand for copper and by the sulphuric acid industry.

The river system is becoming increasingly well characterized as it is a popular location to investigate extremophile microbiology (López-Archilla et al., 2001; Zettler et al., 2002; Gonzalez-Toril et al., 2003a,b; López-Archilla et al., 2004; Aguilera et al., 2007a,b), acid mine drainage processes (Hudson-Edwards et al., 1999; Buckby et al., 2003; Romero et al., 2006; Cánovas et al., 2007, 2008; Gammons et al., 2008), estuarine processes (Elbaz-Poulichet et al., 2001; Braungardt et al., 2003; Olias et al., 2006) and to perform Mars-analogue studies (Fernández-Remolar et al., 2005; Parro et al., 2005; Amils et al., 2007). Fig. 1 shows the headwaters and mining area of the river in detail.

Four site locations in Fig. 1 are of particular interest in this study — Red River, Zarandas Naya (Copper Liquor Dam/Acid River), Tunnel 16 and Tunnel 11. At Red River, a trickle (Q = 0.14 L/s; March 2006) of low pH (1.8 ± 0.25, Aguilera et al., 2007b), concentrated (total Fe (Fe_T) = 304 ± 74 mM, Aguilera et al., 2007b), dark red water flows into one of the headwater streams commonly described as the source of the Río Tinto. The drainage emerges from large waste blocks (~0.5 m) of predominantly acid volcanic tuffs cross-cut by veins containing stockwork pyrite from the Peña del Hierro deposit. Romero et al. (2006) investigated the waste heaps at Peña del Hierro in detail, identifying gossan, shale, roasted pyrite ashes and floated pyrite in addition to the tuffs. They characterized rock fragments and the reactive <2 mm fraction from boreholes and concluded that the tuffs were the main source of acid mine drainage.

The lime green acid mine drainage at Zarandas Naya contrasts strongly with Red River. The valley at Zarandas Naya was the site of heap leaching of approximately 400,000 T of massive pyrite. The heaps were originally 4–10 m in depth and constructed in a terraced manner in a series of valleys, covering an area of approximately 400 acres and capable of holding up to 100,000 m^3 of leachate (Taylor and Whelan, 1942). The leachate was collected at the Copper Liquor Dam (pH = 0.9–1.0, Fe_T = 448–829 mM, this study) and passed through cementation tanks to extract the copper. A visual comparison of the Zarandas Naya heaps suggests that they are much finer grained than the spoil heap at Red River. An analysis of the initial ore used at Zarandas Naya (Taylor and Whelan, 1942) showed it was predominantly pyrite (Table 1). In comparison, analyses of the leached waste by Buckby (2003) showed that it contained quartz, hematite and jarosite in addition to pyrite (Table 1).

Finally, leachate emerging from two underground tunnels, Tunnel 11 (pH = 2.6, Fe_T = 19–27 mM, this study) and Tunnel 16 (pH = 1.1–2.7, Fe_T = 47–195 mM, this study), presents the opportunity to sample acid mine drainage from inaccessible environments for comparison with the first two sites. Tunnel 11 was constructed in several phases (in 1876, 1885, 1900) in order to transport ore from various ore bodies by railway. Drainage from the tunnel emerges from underground and flows in a channel (2–3 m wide) to join the Río Tinto just downstream of Marismilla Reservoir (Fig. 1). Tunnel 16 was completed in 1918 to transport ore from the Corta Atalaya open pit (Fig. 1) and associated underground workings to Zarandas Naya for processing (screening, crushing, heap leaching and cementation).

3. Methods and data validation

3.1. Field sampling and measurements

Water samples were collected from point inputs into the river (Fig. 1 and Table 2) during January, August and November 2003 and April 2004. They were filtered through 0.45 μm nitrocellulose Whatman papers and acidified. pH was measured in the field using a Hanna Instruments meter (HI 8424) with a gel-filled electrode (HI 1230B) and calibrated with buffers at pH 4 and 7. The response of the electrode to samples below pH 4 was evaluated in the laboratory using HCl solutions (pH calculated using the activity coefficients of Hamer and Wu (1972)). These measurements showed that the electrode had a slow response time at low pH and may have overestimated the pH of samples in the field by <0.03 units at pH 2.04, <0.08 units at pH 1.10 and ≥0.2 units at pH 0.09. Eh was measured using a Hanna Instruments meter (HI 8424) with a gel-filled combination platinum, silver:silver chloride electrode (HI 3230B). No measurements were made of ZoBell's solution using the Hanna combination electrode so field Eh readings were corrected to the standard hydrogen electrode using the formula derived from the half-cell potentials in Nordstrom and Wilde (1998) for a silver:silver chloride reference electrode (in 3 M KCl).

Table 1
Mineralogy and chemistry of spoil at Zarandas Naya.

Sample	Initial Ore	TB001255	TB001256	TB001257
Description		Grey waste	Grey/purple waste	Red/purple waste
Mineralogy	py	py, qz, ht, H-jt	py, qz, ht, jt	py, qz, ht, mu
Fe (%)	42	8.25	15.9	24.3
S (%)	47.5	3.65	15.7	10.9
Molar S/Fe	2.0	0.77	1.7	0.77
SiO_2 (%)	5	78.3	50.2	43.2
Cu (ppm)	12500	98	193	743
Zn (ppm)	20000	148	278	1630
Pb (ppm)	15000	3320	7280	17600
As (ppm)	5000	620	1540	1940

Initial ore from Taylor and Whelan (1942), other samples from Buckby (2003). ht = hematite, jt = jarosite, H-jt = hydronium jarosite, mu = muscovite, py = pyrite, qz = quartz.

Table 2
Geochemical and isotopic data.

Location	Grid reference	Sample	Date	T	pH	Eh	Al	As	Ca	Cd	Co	Cr	Cu	Fe	Fe(II)
	UTM 29S			°C		mV	mM	μM	mM	μM	μM	μM	mM	mM	mM
PdH (Upstream)	07161, 41782	CH 24	24/01/03	10.1	2.09	756	1.39	<0.8	0.744	0.064	8.25	0.17	0.009	2.33	0.04
PdH (Red River)	07161, 41782	CH 25	24/01/03	13.5	1.68	841	58.2	57.4	0.384	0.592	214	6.25	0.092	186	2.0
PdH (Lake Doughnut)	07148, 41779	CH 56	26/01/03	10.3	2.06	677	1.23	6.81	0.751	0.419	7.28	0.11	0.051	6.00	<0.001
Tunnel 11	071518, 417441	CH 118	17/08/03	28.3	2.55	663	49.3	8.84	8.13	17.4	278	1.8	7.29	27.4	13
Tunnel 11	071518, 417441	CH 142	26/04/04	24.2	2.66	676	26.5	22.4	4.57	10.1	130	1.0	3.92	19.2	5.2
Tunnel 16	0714940, 4172606	CH 3	23/01/03	22.3	1.09	604	47.1	515	9.08	61.9	178	6.62	4.97	184	154
Tunnel 16	0714940, 4172606	CH 41	24/01/03	22.4	1.35	604	47.4	452	8.86	58.7	193	5.77	5.65	172	133
Tunnel 16	0714940, 4172606	CH 46	25/01/03	22.8	1.41	606	44.5	519	9.56	64.1	161	6.54	4.17	195	159
Tunnel 16	0714940, 4172606	CH 60	26/01/03	22.6	1.28	611	43.4	459	8.81	59.1	190	6.37	4.91	173	133
Tunnel 16	0714940, 4172606	CH 64	13/08/03	22.4	2.47	626	32.1	–	7.39	–	–	–	4.26	79.7	54.8
Tunnel 16	0714940, 4172606	CH 87	15/08/03	–	2.56	–	30.2	–	6.79	–	–	–	3.93	75.7	57.7
Tunnel 16	0714940, 4172606	CH 88	15/08/03	–	2.57	–	35.5	–	6.66	–	–	–	5.87	75.6	61.8
Tunnel 16	0714940, 4172606	CH 89	15/08/03	–	2.67	–	23.1	–	6.16	–	–	–	3.65	70.9	61.8
Tunnel 16	0714940, 4172606	CH 90	15/08/03	–	2.53	–	26.0	–	6.04	–	–	–	3.87	69.8	47.1
Tunnel 16	0714940, 4172606	CH 91	15/08/03	–	2.56	–	29.7	79.0	6.84	24.7	192	1.30	3.81	77.0	59.4
Tunnel 16	0714940, 4172606	CH 108	17/08/03	22.0	2.50	626	28.4	–	6.86	–	–	–	3.60	73.6	59.3
Tunnel 16	0714940, 4172606	CH 133	26/11/03	18.4	2.53	NA	65.0	38.3	4.59	24.5	314	0.75	9.90	46.6	33.3
Tunnel 16	0714940, 4172606	CH 140	26/04/04	20.3	2.72	617	34.0	27.4	5.66	26.6	253	0.73	6.03	53.2	40.8
Settling Pond A	0714870, 4172497	CH 113	17/08/03	20.2	3.25	625	0.121	2.24	3.24	0.0268	4.12	<0.03	0.0005	6.98	6.6
Settling Pond B	0714871, 4172516	CH 47	25/01/03	17.9	2.68	636	9.78	2.94	5.19	0.866	30.2	0.619	0.25	12.4	8.7
Settling Pond B	0714871, 4172516	CH 58	26/01/03	18.9	2.55	632	10.5	1.60	5.39	0.855	29.9	0.608	0.25	14.8	11.4
Settling Pond B	0714871, 4172516	CH 112	17/08/03	34.5	2.40	637	22.1	1.52	12.2	1.57	95.7	1.3	0.27	61.6	51.4
Settling Pond B	0714871, 4172516	CH 141	26/04/04	32.8	2.70	620	21.7	1.41	10.0	1.30	79.8	1.0	0.30	39.9	33.7
ZN (Copper Liquor Dam)	0716067, 4172944	CH 10	23/01/03	13.0	0.88	613	46.0	1260	4.39	14.9	129	21.5	6.48	398	303
ZN (Copper Liquor Dam)	0716067, 4172944	CH 31	24/01/03	15.3	1.00	601	48.6	1230	3.87	16.6	136	21.0	6.67	448	356
ZN (Copper Liquor Dam)	0716067, 4172944	CH 72	13/08/03	31.2	0.96	556	94.9	2780	7.66	33.8	266	37.1	13.4	829	757
ZN (Acid River)	0716033, 4172657	CH 9	23/01/03	20.6	0.92	623	52.3	1130	4.32	17.5	152	24.8	6.89	464	317
ZN (Acid River)	0716033, 4172657	CH 130	26/11/03	10.6	1.26	614	52.3	1900	5.34	13.3	133	25.2	6.00	419	358
ZN (Arroyo Alcojola)	07161, 41726	CH 13	23/01/03	14.8	1.46	643	9.75	226	3.59	2.45	27.7	6.42	1.48	61.1	0.5
ZN (Arroyo Alcojola)	07161, 41726	CH 76	13/08/03	32.3	1.52	616	38.9	571	8.43	9.16	99.3	25.2	6.01	218	172
ZN (Arroyo Alcojola)	07161, 41726	CH 129	26/11/03	11.2	1.48	636	14.6	352	4.19	3.32	37.0	9.15	2.22	91.7	67.7

Location	Sample	K	Mg	Mn	Na	Ni	Pb	Rb	Si	SO_4	Sr	V	Zn	δ^2H	$\delta^{18}O_{H2O}$	$\delta^{18}O_{SO4}$	$\delta^{18}O_{(SO4-H2O)}$
		μM	mM	mM	mM	μM	μM	μM	mM	mM	μM	μM	mM	‰	‰	‰	‰
PdH (Upstream)	CH 24	20	2.92	0.189	0.478	1.98	0.073	0.0139	0.442	9.23	3.40	0.01	0.032	−22.6	−5.0	2.0	7.0
PdH (Red River)	CH 25	33	35.6	0.293	< 0.13	11.0	0.384	0.211	2.41	383	2.40	1.4	0.129	−17.4	−5.1	−1.1	3.9
PdH (Lake Doughnut)	CH 56	67	1.91	0.125	0.439	0.75	0.758	0.0714	0.538	14.9	1.16	0.12	0.161	−20.7	−4.4	1.5	5.9
Tunnel 11	CH 118	49	55.1	3.04	2.33	42.6	0.191	0.226	1.82	191	7.14	0.2	7.28	−23.9	−4.4	0.0	4.4
Tunnel 11	CH 142	56	28.9	1.46	2.07	29.6	0.279	0.114	1.14	101	3.58	3.06	3.96	−19.8	−4.8	1.6	6.3
Tunnel 16	CH 3	610	63.4	2.58	1.60	24.2	13.8	2.56	1.78	424	4.82	24.3	28.9	−27.1	−6.3	6.7	13.1
Tunnel 16	CH 41	690	67.1	2.80	1.54	23.2	12.1	2.30	1.81	408	5.02	21.0	26.8	−23.6	−6.0	6.3	12.3
Tunnel 16	CH 46	790	63.0	2.57	1.62	23.5	14.0	2.64	1.83	424	4.68	24.5	29.5	–	−5.5	8.1	13.6
Tunnel 16	CH 60	560	63.5	2.60	1.44	22.5	11.3	2.22	1.78	392	4.65	22.4	25.1	−24.8	−4.8	7.1	11.9
Tunnel 16	CH 64	–	63.8	2.66	1.19	–	–	–	0.944	228	–	–	12.4	−26.0	−5.4	3.7	9.1
Tunnel 16	CH 87	–	59.5	2.49	1.15	–	–	–	0.869	215	–	–	11.8	−34.3	−5.4	3.4	8.8
Tunnel 16	CH 88	–	65.8	3.04	1.04	–	–	–	0.808	233	–	–	12.4	−25.0	−5.2	2.4	7.6
Tunnel 16	CH 89	–	55.1	2.77	0.935	–	–	–	0.541	189	–	–	11.0	−26.3	−5.6	1.5	7.2
Tunnel 16	CH 90	–	50.2	2.08	0.961	–	–	–	0.879	188	–	–	9.50	−26.6	−5.5	2.3	7.9
Tunnel 16	CH 91	25	60.5	2.49	1.09	22.8	0.613	0.283	0.844	214	4.60	3.73	12.0	−27.3	−5.6	3.3	8.9
Tunnel 16	CH 108	–	58.4	2.40	1.14	–	–	–	0.879	209	–	–	11.1	−27.2	−5.6	2.7	8.3
Tunnel 16	CH 133	61	81.9	3.49	0.613	29.8	1.51	0.215	1.08	263	2.74	0.79	12.3	−23.4	−5.8	−0.5	5.3
Tunnel 16	CH 140	120	56.8	2.84	0.874	32.0	2.19	0.308	0.627	183	4.20	2.34	9.73	−25.3	−5.6	0.1	5.7
Settling Pond A	CH 113	210	7.04	0.346	2.40	20.6	0.030	0.113	0.332	17.9	6.49	0.04	0.113	–	−5.4	0.8	6.2
Settling Pond B	CH 47	100	12.5	0.411	0.565	6.73	0.216	0.0959	1.13	47.1	4.96	0.316	0.506	−24.3	−4.8	0.5	5.2
Settling Pond B	CH 58	110	14.0	0.462	0.613	6.97	0.215	0.0956	1.15	51.7	5.02	0.312	0.560	−28.2	−5.1	0.7	5.8
Settling Pond B	CH 112	250	46.1	1.58	1.76	15.1	0.417	0.429	1.87	164	10.1	0.80	1.85	−19.9	−3.1	−0.1	2.9
Settling Pond B	CH 141	380	33.6	1.14	1.24	12.4	0.647	0.300	1.40	120	8.19	2.30	1.33	−22.0	−4.0	0.9	4.9
ZN (Copper Liquor Dam)	CH 10	1800	14.3	0.868	1.72	33.6	19.2	5.60	0.936	605	2.83	35.1	6.55	−22.3	−6.1	6.0	12.1
ZN (Copper Liquor Dam)	CH 31	1900	14.6	0.916	1.92	31.3	23.1	6.70	1.81	680	2.66	35.5	7.29	–	−5.8	5.5	11.2
ZN (Copper Liquor Dam)	CH 72	4090	28.7	1.80	4.57	92.5	32.8	11.1	2.08	1210	3.16	71.1	16.7	−21.3	−6.6	6.3	13.0
ZN (Acid River)	CH 9	1300	15.9	0.988	2.01	31.5	22.8	6.83	1.76	686	2.86	42.8	7.65	−24.6	−6.2	6.6	12.7
ZN (Acid River)	CH 130	1600	15.1	0.945	1.94	51.6	20.5	5.30	1.50	645	3.05	40.8	7.29	−27.8	−7.0	5.0	12.0
ZN (Arroyo Alcojola)	CH 13	260	5.84	0.457	2.09	12.5	9.03	0.786	1.26	112	3.12	6.24	1.03	−20.9	−5.1	3.6	8.7
ZN (Arroyo Alcojola)	CH 76	360	20.5	1.55	5.96	55.2	17.6	2.57	3.34	369	5.38	31.6	4.71	−19.0	−3.4	3.7	7.1
ZN (Arroyo Alcojola)	CH 129	240	6.91	0.493	2.30	19.1	9.94	0.847	1.35	163	3.16	9.44	1.79	−30.4	−6.2	3.8	9.9

PdH = Pefia del Hierro, ZN = Zarandas Naya.

3.2. Chemical analyses

At the University of Reading, Fe^{2+} concentrations were determined photometrically using a Merck Nova 60 portable spectrophotometer at 522 nm after reaction with 2,2′-bipyridine (Brown et al., 1970). Al, Ca, Cu, total Fe, Mg, Mn, Na S, Si and Zn were analysed using a Perkin Elmer Optima 3000 ICP-OES (Inductively Coupled Plasma — Optical Emission Spectrometer). Reproducibility (1σ) was ±2.8%. As, Cd, Co,

Cr, K, Ni, Pb, Rb, Sr and V were analysed with a Perkin Elmer Elan 6000 ICP-MS (Inductively Coupled Plasma — Mass Spectrometer). Reproducibility (1σ) was $\pm 3.5\%$.

Previous studies from sites in the USA (Nordstrom and Alpers, 1999; Pellicori et al., 2005) and the Iberian Pyrite Belt (Sánchez España et al., 2005) have shown that mine drainage waters typically have sufficient Fe concentrations for the Fe(II)/Fe(III) couple to give an equilibrium potential at the Pt electrode. Measured Eh values were therefore compared with those calculated from the measured iron speciation and full geochemical analyses using PHREEQC (Parkhurst and Appelo, 1999) and the WATEQ4F thermodynamic database (Ball and Nordstrom, 1991). The mean ($\pm 1\sigma$) difference between measured and calculated Eh values was 11 ± 23 mV for 23 out of 25 samples with Eh measurements from this study, indicating good preservation of Fe(II)/Fe(III)_ratios between field sampling in Spain and analysis in the UK. Larger differences were observed for samples CH13 (155 mV difference) and CH56 (229 mV difference), suggesting errors in the field Eh reading or poor sample preservation leading to Fe oxidation subsequent to sampling.

3.3. Stable isotope analyses

Stable isotope analyses were conducted at the Jet Propulsion Laboratory, Pasadena, California, USA using in-line continuous flow techniques and a Thermo Finnigan Mat 253 Isotope Ratio Mass Spectrometer (IRMS). δ^2H_{H2O} was determined by introducing the water sample into a Thermo Finnigan H-Device before transfer to the IRMS (Spangenberg et al., 2007; Smuda et al., 2008). For $\delta^{18}O_{H2O}$, the sample was equilibrated with CO_2 for 24 h (Epstein and Mayeda, 1953) in a Finnigan GasBench II before transfer to the IRMS (Spangenberg et al., 2007; Smuda et al., 2008).

Sulphate for $\delta^{18}O_{SO4}$ analyses was prepared by dilution of a sample, containing sufficient sulphate to obtain 50 mg of $BaSO_4$, in a total volume of 30 ml 0.05 M HCl. It was precipitated as $BaSO_4$ by the dropwise addition of 0.2 M $BaCl_2$ to the near-boiling, acidified solution, which was then maintained at 70 °C for 1 h to encourage formation of a coarser precipitate (Kolthoff et al., 1969; Vogel and Jeffery, 1989). Our aim was to minimise the extent of sample handling but to avoid analytical artifacts. The $BaSO_4$ was washed in distilled deionised water and dried in air at 100 °C but was not processed further. Our trials of preparation methods indicated that the possible trapping of water in the dried precipitate would have a negligible effect on measured oxygen isotope values. We made a comparison with drying at 500 °C and showed that the proportion of oxygen contributed by water was less than 0.3%, which we confirmed by precipitation of $BaSO_4$ from water enriched in ^{18}O. Clearly, this has a negligible effect on the measured values of our samples relative to analytical error. Similarly, we tested the possible effects of precipitation from an iron-rich solution by twice dissolving $BaSO_4$ precipitates in DTPA and re-precipitating them (Bao, 2006). In all cases tested we found average apparent differences that were not consistent in sign and less than analytical error. 200 μg of $BaSO_4$ was loaded in a Ag cup, converted to CO in a Thermo Finnigan TC/EA at 1450 °C and passed directly through a Conflo III system into the IRMS (Knoller et al., 2004; Balci et al., 2007; Lefticariu et al., 2007).

Certified reference materials from IAEA (V-SMOW, SLAP and GISP) and NIST (NBS18, NBS19, NBS30 and NBS127) were run as samples and used to calibrate the data. Reproducibility (1σ) was $\pm 1.3‰$ for δ^2H, $\pm 0.3‰$ for $\delta^{18}O_{H2O}$ and $\pm 0.4‰$ for $\delta^{18}O_{SO4}$. This reproducibility is sufficient for the purpose of this study. Stable isotope data are expressed in delta (δ) notation as parts per thousand (‰) relative to the Vienna Standard Mean Ocean Water (V-SMOW).

3.4. Geochemical modelling

Geochemical modelling was performed using the full geochemical analyses given in Table 2, PHREEQC for Windows version 2.12.02 (Parkhurst and Appelo, 1999; graphic user interface by V.E.A Post,

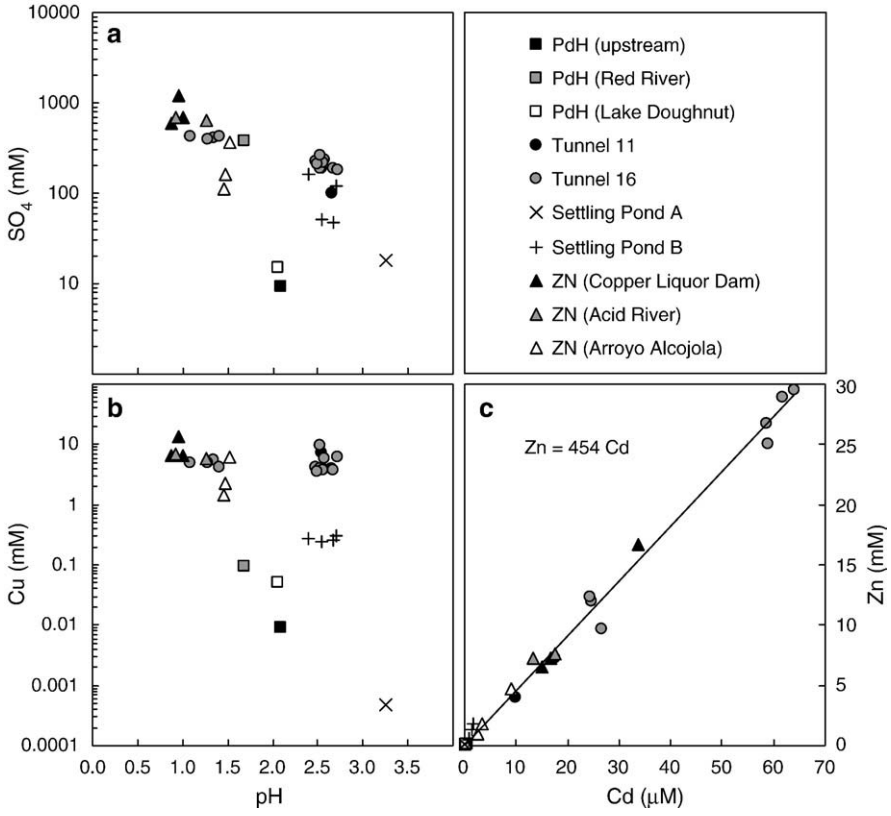

Fig. 2. Chemistry of Río Tinto point inputs: (a) SO_4 vs. pH. (b) Cu vs. pH. (c) Zn vs. Cd.

2005) and the WATEQ4F thermodynamic database (Ball and Nordstrom, 1991; PHREEQC file details: "wateq4f.dat 431 23/08/05"). The solubility products for mineral phases presented in this study were taken from WATEQ4F and Chapman et al. (1983; plumbojarosite, $Pb_{0.5}Fe_3(SO_4)_2(OH)_6$, $\log K_{sp} = -8.14$). Redox information was taken from measured Fe^{2+} and Fe^{3+} data.

4. Results

Table 2 summarises the data for the point inputs sampled in this study, highlighting the variations in pH (0.88–3.25), aqueous concentrations (e.g. $Fe_T = 2.3$–829 mM) and sulphate–oxygen isotopes ($\delta^{18}O_{SO4} = -1.1$ to 8.1‰). The samples with the lowest pH and highest dissolved sulphate and metal concentrations emanated from the heap leaching waste at Zarandas Naya (Fig. 2). Fig. 2 shows that despite high dissolved sulphate concentrations (383 mM), the drainage at Red River contained low concentrations of metals other than Fe (e.g. Cu = 0.09 mM). Drainage from the settling ponds also contained relatively low concentrations of metals (Cu < 0.3 mM, Zn < 2 mM). Figs. 2 and 3 show temporal variations in the chemistry of Tunnel 16, with the pH increasing and sulphate concentrations and $\delta^{18}O_{SO4}$ decreasing after January 2003.

5. Discussion

5.1. Sources of dissolved sulphate

Fig. 2c shows a linear relationship between Zn and Cd concentrations. The Zn/Cd ratio of 454 is within the range reported for Cd in sphalerite (Fuge et al., 1993), suggesting that sphalerite oxidation is

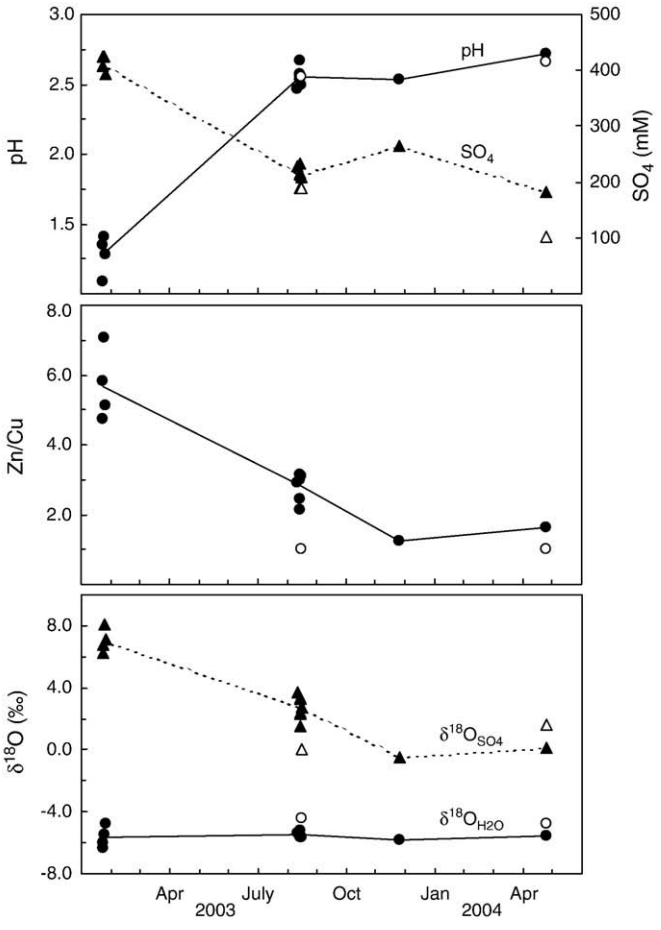

Fig. 3. Temporal variations in the drainage chemistry of Tunnel 16 (closed symbols) and Tunnel 11 (open symbols).

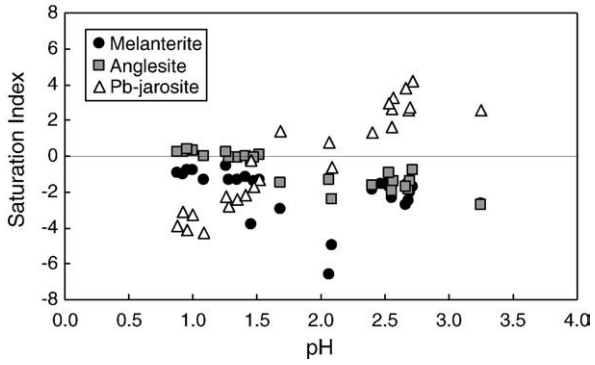

Fig. 4. Saturation indices of melanterite, anglesite and plumbojarosite.

the primary control on dissolved Cd. However, Cd is a minor component of the waters with Fe, Cu and Zn comprising 99.6 ± 0.2% (mean ± σ, $n = 25$) of the molar total of sulphide-derived metals (As, Cd, Co, Cu, Fe, Ni, Pb, Zn) in the acid mine drainage point inputs. A mass balance approach, Eqs. (4)–(7) can therefore be used to examine variations in the sulphide sources assuming that total dissolved S (S_T) is derived from pyrite (py; FeS_2), chalcopyrite (cp; $CuFeS_2$) and sphalerite (sp; ZnS). However, sulphate could also be derived from soluble sulphate minerals, such as gypsum/anhydrite, $CaSO_4(.2H_2O)$. An examination of Ca/SO_4 molar ratios shows that 82% (27 out of 33) of the samples in Table 2 have Ca/SO_4 ratios ≤0.05 and 100% have ratios <0.2, suggesting that most of the sulphate is derived from sulphide oxidation rather than gypsum dissolution.

$$S_T = S_{py} + S_{cp} + S_{sp} \quad (4)$$

$$S_{cp} = Cu + Fe_{cp} = 2\ Cu \quad (5)$$

$$S_{py} = 2Fe_{py} = 2(Fe_T - Fe_{cp}) = 2(Fe_T - Cu) \quad (6)$$

$$S_T = 2(Fe_T - Cu) + 2Cu + Zn = 2Fe_T + Zn \quad (7)$$

The contribution of hydrated iron sulphate minerals (e.g. melanterite, $FeSO_4.7H_2O$) also needs to be considered. These minerals generally form from concentrated, evaporating waters and can be found on the riverbanks and spoil heaps during summer periods. Dissolution of these minerals occurs with the first rainfall events of the autumn/winter (Cánovas et al., 2008). However, the winter sampling in January and November 2003 occurred after these dissolution events. Geochemical modelling predicts that the waters are undersaturated with respect to melanterite (Fig. 4), the first ferrous sulphate mineral to form (Jambor et al., 2000), implying that these minerals form from evaporating pore waters/stagnant pools rather than the bulk waters sampled in August 2003.

The removal of Fe from solution as Fe-oxyhydroxy(sulphate) ochreous phases such as jarosite and schwertmannite would increase the relative contributions of Zn and Cu, giving a false impression of the sulphide ores leached by these waters. Eq. (8), rearranged from Eq. (7), calculates the theoretical dissolved Fe concentrations (Fe_{calc}), assuming that Cu and Zn behave conservatively. This theoretical value can then be compared with the measured Fe value, Fe_{meas} (Eq. (9), negative values show calculated % of Fe removed from solution).

$$Fe_{calc} = (S - Zn)/2 \quad (8)$$

$$\Delta Fe(\%) = 100x(Fe_{meas} - Fe_{calc})/Fe_{calc} \quad (9)$$

Fig. 5 shows a plot of ΔFe vs. pH. The only samples that approximate congruent sulphide dissolution with no Fe ochre precipitation are the low pH waters from Red River and the Tunnel 16

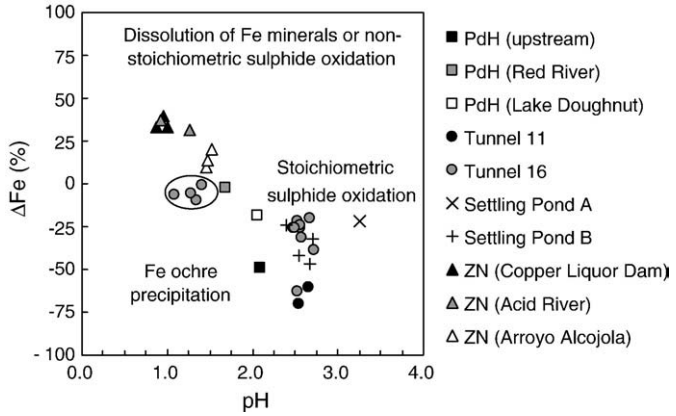

Fig. 5. Processes controlling dissolved Fe concentrations. Ringed Tunnel 16 samples from January 2003.

waters sampled in January 2003. The rise in pH of Tunnel 16 after January 2003 (Fig. 3) was accompanied by ochre precipitation (Fig. 5 and visual observations). Leachate from Zarandas Naya had 9–39% more Fe than can be explained by sulphide oxidation alone. This could be due to preferential leaching of Fe, which has been used to explain experimental pyrite oxidation results (e.g. Sasaki et al., 1995; Yu et al., 2001). Descostes et al. (2004) suggested an alternative mechanism (based on Luther, 1997) involving the release of a reduced sulphur compound to solution, which then disproportionates e.g. thiosulphate to S^0 and tetrathionate. The S^0 then accumulates on the pyrite surface (Sasaki et al., 1995; Schippers et al., 1999; McGuire et al., 2001; Druschel and Borda, 2006) and the solution is enriched in Fe relative to S. However, Druschel and Borda (2006) noted that the slow oxidation kinetics of tetrathionate by Fe^{3+} and O_2 in acidic conditions (compared with thiosulphate oxidation to tetrathionate, Druschel et al., 2003a) would lead to the accumulation of tetrathionate in solution, which was not observed by Descostes et al. (2004). Descostes et al. (2004) and Brunner et al. (2008) also suggested partial disproportionation to SO_2 to give low S/Fe ratios. Preferential leaching of Fe would leave a solid phase enriched in S. However, all three samples analysed by Buckby (2003) were enriched in Fe (S/Fe ≤1.7; Table 1). The waste also contained hematite and jarosite so the low aqueous S/Fe ratios could be due to low pH leaching of these minerals or residual felsic volcanic gangue material (Taylor and Whelan, 1942) rather than non-stoichiometric pyrite leaching.

Having estimated iron precipitation it is now possible to estimate the relative percentages (by mass) of Fe, Cu, Zn and S (total = 100%) leached from the original sulphide ore using Fe_{calc}, Cu and Zn concentrations. Fig. 6 compares these values between different sources and with reported analyses of sulphide ore from the Río Tinto (Taylor and Whelan, 1942; Tornos, 2006). The samples from Zarandas Naya and some of the samples from the settling ponds and Peña del Hierro fall within the analysed range. These calculations also highlight the dominance of pyrite oxidation, particularly for the waste sulphides leached at Peña del Hierro.

The higher Cu and Zn percentages in the tunnel inputs compared with Cu and Zn grades in the ore indicate that these elements are being leached preferentially. This agrees with observations by Taylor and Whelan (1942) that >75% of the Cu and Zn were leached from the heaps at Zarandas Naya within the typical lifetime of a heap, compared with 19% of the Fe. These observations can be explained by galvanic protection of the pyrite (Kwong et al., 2003), where sphalerite and chalcopyrite have lower electrode potentials than the pyrite they are in contact with and act as anodes, leading to the enhanced release of Cu and Zn. The higher Cu and Zn values for Tunnel 16 and Tunnel 11 compared with Zarandas Naya suggests that the tunnel inputs have access to comparatively fresh ore while the heaps at Zarandas Naya contain highly weathered material. The age of the material currently in the heaps is unknown but is likely to be decades old. Note the temporal variation of Cu and Zn in Tunnel 16 (Figs. 3 and 6), suggesting a change to a drainage source more similar to that of Tunnel 11.

A galvanic protection mechanism for pyrite would also release Pb into solution since galena (PbS) has a lower electrode potential than pyrite. Although Pb is present at similar concentrations to Cu and Zn in the initial pyritic ore (Table 1), it has much lower dissolved concentrations in the acid mine drainage (Zn = 0.03–30 mM, Pb = 0.03–33 μM). Equilibrium modelling predicts that Pb concentrations are limited by equilibrium with anglesite ($PbSO_4$) below pH 1.5 and by the precipitation of plumbojarosite ($Pb_{0.5}Fe_3(SO_4)_2(OH)_6$, $\log K_{sp} = -8.14$; Chapman et al., 1983) or the incorporation into a mixed jarosite phase (Hochella et al., 1999) above this pH (Fig. 4).

5.2. Sulphide oxidation pathways determined from oxygen isotopes

Several models have been proposed in the literature for interpreting oxygen isotope data. The range of $\delta^{18}O_{SO4}$ values (−1.1 to 8.1‰) in the Río Tinto point inputs are an excellent opportunity to compare these models with each other and with published pathways for sulphide and sulphoxyanion oxidation. Firstly, the stoichiometric isotope balance model (Eq. (10), where X is the fraction of sulphate derived from Eq. (3) and $(1-X)$ is the fraction derived from Eq. (1); Taylor et al., 1984a,b; van Everdingen and Krouse, 1985) describes the oxygen isotope data in terms of the familiar pyrite oxidation equations with either molecular oxygen (Eq. (1)) or ferric iron (Eq. (3)) as the oxidants. This model is attractive in its simplicity and has been used to interpret field data (Taylor and Wheeler, 1994; Butler, 2007).

$$\delta^{18}O_{SO4} = X(\delta^{18}O_{H2O} + \varepsilon_{H2O}) + (1-X)[0.875(\delta^{18}O_{O2} + \varepsilon_{O2}) + 0.125(\delta^{18}O_{H2O} + \varepsilon_{H2O})] \quad (10)$$

A criticism of the stoichiometric isotope balance model is that it does not sufficiently describe the intermediate steps involved in pyrite oxidation. The general isotope balance model (Eq. (11), where Y is the fraction of sulphate–oxygen derived from water; Taylor and Wheeler, 1994) is a more flexible approach than the stoichiometric model and is currently the most popular approach applied to field data (Haubrich and Tichomirowa, 2002; Knoller et al., 2004; Sracek et al., 2004; Migaszewski et al., 2008): it also uses oxygen and water fractionation factors derived from experiments but gives relative proportions of oxygen sources (rather than end-member equations), which can then be used to constrain potential reaction pathways.

$$\delta^{18}O_{SO4} = Y(\delta^{18}O_{H2O} + \varepsilon_{H2O}) + (1-Y)(\delta^{18}O_{O2} + \varepsilon_{O2}) \quad (11)$$

Neither of these models accounts for isotope exchange reactions. The sulphite-water oxygen exchange model of Seal (2003) has two

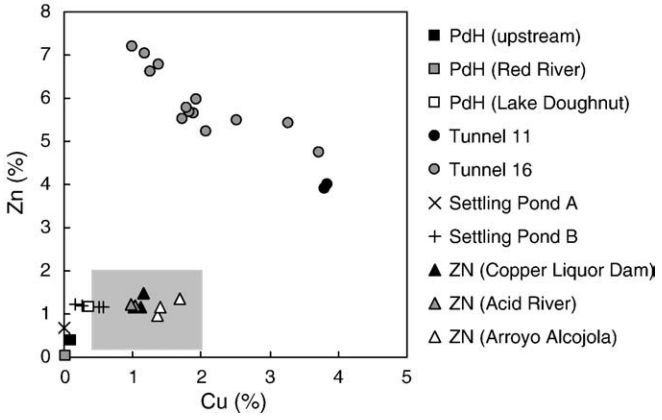

Fig. 6. Relative % of Cu and Zn released into solution from sulphide oxidation (Fe + Cu + Zn + S = 100%).

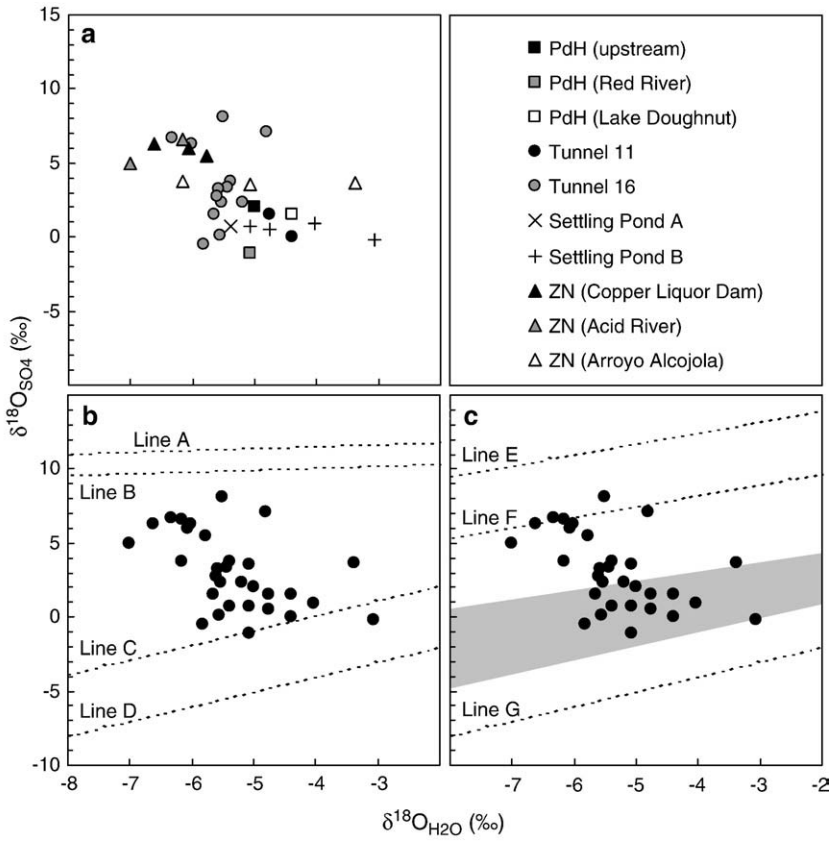

Fig. 7. Oxygen isotope data: (a) Site specific data. (b) Stoichiometric isotope balance model. Line A ($\varepsilon_{H2O} = 3.3‰$, $\varepsilon_{O2} = -10.2‰$) and Line B ($\varepsilon_{H2O} = 0‰$, $\varepsilon_{O2} = -11.4‰$) represent 100% input from Eq. (1). Line C ($\varepsilon_{H2O} = 4.1‰$) and Line D ($\varepsilon_{H2O} = 0‰$) represent 100% input from Eq. (3). (c) Sulphite–water oxygen exchange model. Line E ($\delta^{18}O_{SO4} = 0.74\ \delta^{18}O_{H2O} + 15.4$; oxygen-limited conditions) and Line F ($\delta^{18}O_{SO4} = 0.72\ \delta^{18}O_{H2O} + 11.1$; oxygen-unlimited conditions) represent 100% release as intermediate sulphoxyanion, followed by sulphite–water oxygen exchange and oxidation to sulphate by O_2. Line G ($\delta^{18}O_{SO4} = \delta^{18}O_{H2O}$) represents 100% direct release of sulphate from the pyrite surface. Shaded area represents data from pyrite oxidation experiments where the proportion of water–oxygen was determined explicitly.

end-members: firstly, the direct release of sulphate from the pyrite surface, incorporating 100% water–oxygen with $\varepsilon_{H2O} = 0‰$ and secondly, the release of intermediate sulphoxyanions followed by their oxidation to sulphate via sulphite, sulphite–water oxygen exchange and sulphite oxidation to sulphate by O_2. Predicted $\delta^{18}O_{SO4}$ values for the second end-member were based upon experiments by Holt et al. (1981) on the aqueous phase oxidation of SO_2 (i.e. HSO_3^- or SO_3^{2-}) under oxygen-limited conditions in the presence of Fe^{3+} ($\delta^{18}O_{SO4} = 0.74\ \delta^{18}O_{H2O} + 15.4$; curve A from Holt et al., 1981) and oxygen-unlimited conditions ($\delta^{18}O_{SO4} = 0.72\ \delta^{18}O_{H2O} + 11.1$; curve G from Holt et al., 1981), with sulphite being oxidized to sulphate by atmospheric oxygen.

Fig. 7 summarizes the oxygen isotope data from the Río Tinto. Modelling results are given in Table 3. For the stoichiometric isotope balance model and the general isotope balance model, three sets of fractionation factors were used: (i) $\varepsilon_{H2O} = 4.1‰$ and $\varepsilon_{O2} = -11.4‰$ (Taylor et al., 1984b); (ii) $\varepsilon_{H2O} = 0‰$ and $\varepsilon_{O2} = -11.4‰$ (Taylor and Wheeler, 1994); (iii) $\varepsilon_{H2O} = 3.3‰$ and $\varepsilon_{O2} = -10.2‰$ (average values from Balci et al., 2007). The biotic value of ε_{O2} from Taylor et al. (1984b) was chosen as *A. ferrooxidans* has been identified in mine waters from the Río Tinto (Gonzalez-Toril et al., 2003a) and this value is also close to the values determined more recently by Balci et al. (2007), who found similar fractionation factors for abiotic and biotic experiments ($\varepsilon_{O2} = -9.8$ to $-10.8‰$).

Table 3
Quantification of pyrite oxidation pathways.

	εH_2O (‰)	εO_2 (‰)	All data	Red River	CLD/AR	Tunnel 16
Stoichiometric isotope balance model			% sulphate from Eq. (3)			
Taylor et al. (1984b)	4.1	−11.4	20–112	101	30–41	20–90
Taylor and Wheeler (1994)	0	−11.4	12–78	74	20–28	12–66
Balci et al. (2007)	3.3	−10.2	24–103	95	33–43	24–85
General isotope balance model			% water–oxygen in sulphate			
Taylor et al. (1984b)	4.1	−11.4	30–111	101	39–48	30–91
Taylor and Wheeler (1994)	0	−11.4	23–81	77	30–37	23–70
Balci et al. (2007)	3.3	−10.2	34–103	96	42–50	34–87
Sulphite–water oxygen exchange model			% released as intermediate sulphoxyanions			
Oxygen limited conditions	0	–	18–81	24	66–76	31–81
Oxygen unlimited conditions	0	–	24–108	32	88–100	42–108

CLD/AR = Copper Liquor Dam/Acid River.

Applying the stoichiometric isotope balance approach to the Río Tinto dataset gives a range of 20–112% input from ferric iron oxidation ($\varepsilon_{H2O} = 4.1‰$ and $\varepsilon_{O2} = -11.4‰$). The value over 100% (sample CH111) may be due to evaporation subsequent to pyrite oxidation increasing the value of $\delta^{18}O_{H2O}$. Fig. 8 compares the water isotopes with the Western Mediterranean Meteoric Water Line (WMMWL; $\delta_2H = 8\delta^{18}O_{H2O} + 13.7$, $n = 146$, Celle-Jeanton et al., 2001). Most of the data plots to the left of the WMMWL but there is an insufficient range of data to draw a local meteoric water line. The importance of evaporation in modifying water isotopes and concentrating waters is shown by samples taken from the river channel itself in August 2003 (Fig. 8a). A smaller degree of evaporation cannot therefore be ruled out for some of the point inputs (Fig. 8b) as the data show possible parallel trends to the illustrated evaporation line. Alternatively, the high value may indicate that the chosen ε_{H2O} is too high. Based on field data, Taylor and Wheeler (1994) proposed that $\varepsilon_{H2O} = 0‰$. This gives a range of 12–78% of sulphate derived from pyrite oxidation by ferric iron. Table 3 and Fig. 7b highlight the difference that varying ε_{H2O} and ε_{O2} values makes on the quantification of pyrite oxidation pathways.

5.2.1. Red River

At the Red River site location (CH25, pH = 1.7, Fe_T = 186 mM; January 2003), pyrite oxidation dominates the isotopic signature and it occurs congruently i.e. sulphide is fully oxidized to sulphate (Fig. 3). Concentrations were lower than measured by Aguilera et al. (2007b), most likely as a result of dilution by winter rainfall events, although higher concentrations (e.g. Fe_T = 406 mM, September 2004) have been measured during the dry summer. Fe speciation is >98% Fe(III) and microbiological studies at the site have identified Fe-oxidizing bacteria (*Leptospirrilum ferriphilum* and *A. ferrooxidans*; Gonzalez-Toril et al., 2003a), suggesting that pyrite is oxidized by ferric iron, which is maintained by an active population of microbes. This hypothesis is supported by the oxygen isotope data and the stoichiometric isotope balance model; the small difference of 4‰ between $\delta^{18}O_{SO4}$ and $\delta^{18}O_{H2O}$ corresponds to 74–101% (depending on the fractionation factors used, see Table 3) of pyrite oxidation by ferric iron (Eq. (3)) rather than atmospheric oxygen. Note that 4‰ is close to the water fractionation factors suggested by Taylor et al. (1984a,b; 4.1‰) and Balci et al. (2007; 3.3‰).

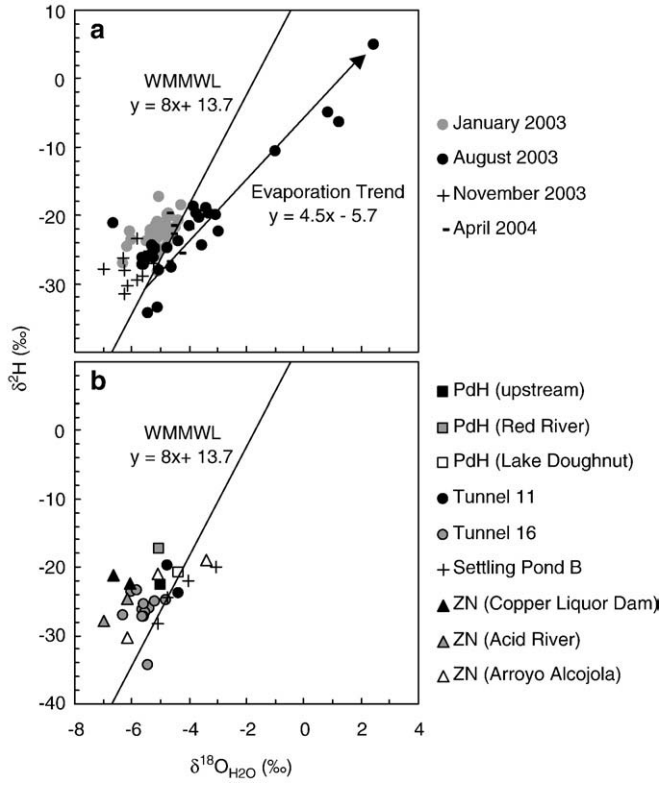

Fig. 8. Water isotopes. WMMWL = Western Mediterranean Meteoric Water Line. (a) Seasonal datasets from the river channel and point inputs. (b) Site specific data.

In contrast to the reasoning behind the stoichiometric balance model, a recent model of pyrite oxidation by Rimstidt and Vaughan (2003) suggests that water–oxygen rather than atmospheric oxygen interacts with the S-moiety on the pyrite surface, irrespective of the oxidant (O_2 or Fe^{3+}). They proposed an electrochemical model consisting of a cathodic site (where an electron is transferred to Fe^{3+}/O_2 from the Fe^{2+} in the mineral surface), an anodic site (where the S-moiety is oxidized) and electron transport from the anodic to the cathodic site. Continued electron transport from the anodic site withdraws more electrons from the terminal S and allows continued hydrophilic attack by water molecules. Spectroscopic studies and ab initio calculations (Nesbitt and Muir, 1994; Rosso et al., 1999) have shown that Fe oxidation precedes S oxidation on the pyrite surface, with water and oxygen initially dissociatively sorbing to Fe dangling bonds on the pyrite surface rather than S sites. This leaves the S sites more electropositive (Rosso et al., 1999; Rimstidt and Vaughan, 2003), allowing nucleophillic attack by the negative end of the water dipole, or by hydroxyl radicals produced from water at the pyrite surface (Moses et al., 1987; Borda et al., 2003a).

Balci et al. (2007) proposed that oxygen isotope fractionation is most likely to occur during the transfer of an oxygen atom from the hydroxyl radical of the aqua-Fe(III) complex to the S-moiety of pyrite. This process could therefore explain the isotopic signature of Red River, with microbially produced ferric iron as the oxidant and the direct release of sulphate into solution from the pyrite surface. Brunner et al. (2008) also showed that during the main stage of biotic pyrite oxidation experiments at pH 1.8–2.1, *A. ferrooxidans* in exponential growth phase leached pyrite almost congruently (S/Fe = 1.9), with ferric iron as the dominant iron species, producing sulphate with a similar oxygen isotope signature to water.

5.2.2. Zarandas Naya

At Zarandas Naya, water flowing through the fine-grained heaps is continually exposed to pyrite, explaining why the iron speciation analysed from the Copper Liquor Dam was predominantly ferrous (76–91%). The drainage that emerged at the Copper Liquor Dam and flowed down to meet the river channel at Acid River was even more concentrated than Red River (Fe_T = 398–829 mM) with a lower pH (0.88–1.26). Given the slow response of the pH meter to low pH, these measurements could be 0.08–0.2 units too high. The half-life of sulphate–water oxygen exchange at pH 0.7 is approximately 210 years at 25 °C (Hoering and Kennedy, 1957; Chiba and Saki, 1985; Seal, 2003), implying that this is not a significant mechanism for altering $\delta^{18}O_{SO4}$ values. The only scenario where this could take place would be if pyrite oxidation mainly occurred in thin, concentrated films within/coating pyrite crystals in the unsaturated zone and was then diluted and transported to the saturated zone following rainfall events. However, as described above, this would require extremely low pH solutions and such pore waters have not yet been sampled from within the heaps.

The oxygen isotope data at Copper Liquor Dam and Acid River also contrast strongly with Red River. The values of $\delta^{18}O_{(SO4-H2O)}$ were 11.2–13.0‰. This equates to 57–80% of oxidation via Eq. (1), according to the stoichiometric isotope balance model and 50–70% of O_2-derived rather than water-derived sulphate–oxygen, according to the general isotope balance model (Table 3). If only water–oxygen interacts with the pyrite S-moiety (Rimstidt and Vaughan, 2003), then atmospheric oxygen must be incorporated into sulphate during the oxidation of dissolved sulphoxyanion intermediates. Thiosulphate is commonly suggested as the species released into solution from the pyrite surface (e.g. Goldhaber, 1983; Luther, 1987; Moses et al., 1987; Schippers et al., 1996). Based on the results of their short-term aerobic experiments and the reaction pathway suggested by Schippers et al. (1996), Balci et al. (2007) proposed Eq. (12) as the overall reaction of pyrite

oxidation via thiosulphate, with sulphate being formed from the hydrolysis of tetrathionate and the O_2 oxidation of sulphite. This gives 12.5% of sulphate–oxygen derived from O_2.

$$2FeS_2 + 12Fe(H_2O)_6^{3+} + 19H_2O + 2Fe^{3+} + 0.5O_2 \rightarrow 14Fe(H_2O)_6^{2+} + 2Fe^{2+} + 14H^+ + 2SO_4^{2-} + 0.2S_8 \quad (12)$$

This pathway cannot explain the incorporation of 50–70% atmospheric oxygen into the Copper Liquor Dam/Acid River waters, according to the general isotope balance model. Druschel et al. (2003a) conducted abiotic oxidation experiments of thiosulphate and polythionates at pH 0.5–2.0 under various combinations of Fe^{3+} and O_2. The average reaction was represented by Eq. (13). Assuming that all the oxygen in the tetrathionate was derived from water and that there is no isotopic exchange with it, this gives a final sulphate containing only 34% atmospheric oxygen.

$$S_4O_6^{2-} + 3Fe^{3+} + 2.75O_2 + 4.5H_2O \rightarrow 4SO_4^{2-} + 3Fe^{2+} + 9H^+ \quad (13)$$

Furthermore, Druschel et al. (2003a) noted that the slow kinetics of tetrathionate oxidation to sulphate by Fe^{3+} and O_2 relative to its formation would lead to it accumulating in solution. Tetrathionate oxidation by hydroxyl radicals is at least 14 orders of magnitude faster than oxidation by Fe^{3+} or O_2 (Druschel et al., 2003b) and may pass through a possible $S_3O_4^{n-}$ intermediate but this pathway is currently poorly constrained. Hydroxyl radicals and H_2O_2 may be produced from water at defect sites following wetting of the pyrite surface or by photochemical induced electron-hole pair formation (Borda et al., 2003a). Reaction with these species will therefore incorporate water–oxygen in the sulphoxyanion. Lowson (1982) proposed a Fenton-type mechanism for O_2 reduction by Fe^{2+} at the pyrite surface, which would incorporate O_2-oxygen into OH* and H_2O_2, although Rimstidt and Vaughan (2003) suggested that hydroxide ions (containing O_2-oxygen) would be the species released back to solution. Further work is needed to quantify the relevance of reactions with hydroxyl radicals and H_2O_2 compared with Fe^{3+} and O_2 (e.g. Lefticariu et al., 2007).

The dominance of ferrous iron in the Río Tinto samples with high $\delta^{18}O_{(SO4-H2O)}$ also suggests that the pathway in Eq. (13) may be limited at these sites by the oxidation of ferrous iron. If ferric iron is a limiting factor, then thiosulphate disproportionation to bisulphite and elemental sulphur may occur (Eq. (14)). The bisulphite could then be oxidized to sulphate by O_2, Fe^{3+} or a hydroxyl radical (Huie and Neta, 1987; Ermakov et al., 1997; Brandt and van Eldik, 1998), resulting in 75–100% water–oxygen in the final sulphate.

$$S_2O_3^{2-} + H^+ \rightarrow HSO_3^- + S_0 \quad (14)$$

It is important to note that none of these proposed pathways can explain the high percentage of atmospheric oxygen predicted by the general isotope balance model in the Copper Liquor Dam/Acid River waters. A possible explanation would be if O_2 interacted directly with the S-moiety on the pyrite surface (Luther, 1987). This mechanism is currently not favoured in the literature but could help explain high $\delta^{18}O_{(SO4-H2O)}$ values from field studies.

A further problem with pathways involving thiosulphate is that recent papers have questioned its release at low pH. Rimstidt and Vaughan (2003) argued that at high pH the terminal S is completely ionized, making the S–S bond stronger than the Fe–S bond and promoting $S_2O_3^{2-}$ release. In contrast, they argued that at low pH the terminal S is protonated (Fe–S–SO_3H) encouraging electron transfer to the S–S bond and then to the cationic site, making the terminal S very electropositive leading to a fourth nucleophillic attack by water and the formation of sulphate. Borda et al. (2003b) used ATR-FTIR spectroscopy to examine species on the pyrite surface at pH 2.0. They found that thiosulphate-like moieties were present as monodentate inner sphere complexes rather than outer sphere complexes whereas sulphate was present as an outer sphere ion and concluded that sulphate rather than thiosulphate was the surface-release group. The spectral resolution could not rule out the possibility of a sulphite-like species on the pyrite surface (Druschel and Borda, 2006), which could also be the species released into solution. Pyrite oxidation experiments in the laboratory have only directly detected dissolved thiosulphate above pH 7 (Goldhaber, 1983; Moses et al., 1987; Schippers et al., 1996), although Schippers et al. (1996) used an indirect technique (precipitation by adding $AgNO_3$) to show that 78% of the total S was released as thiosulphate at pH 1.7 in the presence of excess Fe^{3+}. Note that sulphite also forms an insoluble precipitate with Ag^+ ions so this result is not conclusive of thiosulphate release.

An alternative approach to interpreting oxygen isotope data focuses on the role of dissolved sulphite (Seal, 2003). Sulphite is commonly proposed as a precursor to sulphate in both abiotic and biotic oxidation pathways (Suzuki et al., 1994; Schippers et al., 1996; Kelly, 1999; Schippers et al., 1999; Druschel et al., 2003a,b). Betts and Voss (1970) showed that dissolved sulphite rapidly exchanges oxygen with water (half-life, $t(1/2) = 25.3$ h at pH 10.5 and 1.3 min at pH 8.9). Assuming a linear relationship between pH and log $t(1/2)$ (compare with sulphate–water oxygen exchange kinetics; Seal, 2003), this predicts half-lives of 18 ms at pH 7 and 4.6×10^{-12} s at pH 2. Hence at low pH, all of the oxygen in dissolved sulphite may be in equilibrium with and effectively derived from water, irrespective of the source of oxygen involved in previous oxidation steps. Sulphite–water oxygen exchange results in a positive fractionation such that $\delta^{18}O_{SO3} = \delta^{18}O_{H2O} + X$. Brunner et al. (2006) determined X at pH 7.2 ($X = 12.7 \pm 1‰$ at 4 °C, $11.5 \pm 1‰$ at 23 °C and $10.3 \pm 1‰$ at 70 °C) and at pH 8 ($X = 9.8 \pm 1‰$ at 4 °C, $7.9 \pm 1‰$ at 23 °C and $6.0 \pm 1‰$ at 70 °C). The apparent change in fractionation with pH could have resulted from a change in sulphoxyanion speciation, with the value at higher pH relating to a part of the phase diagram where sulphite ion is the predominant species as opposed to more HSO_3^- at neutral pH. It would be useful to check this by repeating the experiments at lower pHs, such as those relevant to the Río Tinto system.

Applying the sulphite–water oxygen exchange model of Seal (2003) suggests that the majority of the sulphate (66–100%) in the low pH, ferrous iron waters of the Copper Liquor Dam/Acid River was released as intermediate sulphoxyanions and oxidized via sulphite rather than being released directly as sulphate. The proportion varies depending on the end-member equation used from Holt et al. (1981), with 88–100% predicted under oxygen-unlimited conditions compared with 66–76% under oxygen-limited conditions. The spoil heaps at Zarandas Naya were originally constructed to encourage ingress of O_2 (Taylor and Whelan, 1942), although it is conceivable that subsequent changes in the heaps' mineralogy and permeability may have decreased oxygen introduction rates.

A complication to the model is that ferric iron can also oxidize sulphite (Brandt and van Eldik, 1998; Millero, 2001). According to the relative abundances and reaction rates of O_2 and Fe^{3+}, the fourth oxygen in sulphate could originate from O_2 (giving $S(O_w)_3O_a^{2-}$) or water (giving $S(O_w)_4^{2-}$). Assuming that equilibrium exchange results in sulphite with $\delta^{18}O_{(SO3-H2O)} = 11.5 \pm 1‰$ (the lower pH value from Brunner et al., 2006), this predicts $\delta^{18}O_{(SO4-H2O)}$ values of 7.9–10.4‰ with Fe^{3+} as the oxidant (and $\varepsilon_{H2O} = 0$ to 4.1‰) and 10.9–12.7‰ with O_2 as the oxidant (and $\varepsilon_{O2} = -10.2$ to $-11.4‰$). The acid mine drainage from Copper Liquor Dam/Acid River had $\delta^{18}O_{(SO4-H2O)}$ values of 11.2–13.0‰, suggesting that O_2 was the oxidant.

The release of sulphite from the pyrite surface would be consistent with the oxygen isotope data for Copper Liquor Dam/Acid River (allowing sulphite–water isotopic exchange to occur) and with the oxidation scheme of Rimstidt and Vaughan (2003), which argues that the S–S bond rather than the Fe–S bond of the S-moiety on the pyrite surface is broken at low pH. It would also leave a monosulphide group at the surface, which could be abiotically or biotically oxidized to sulphate via polysulphides, S^0 and through a sulphite intermediate

(Suzuki et al., 1994; Schippers et al., 1999; Druschel and Borda, 2006). Incomplete oxidation via the monosulphide route would give dissolved S/Fe molar ratios below 2 and may leave a S^0 enriched surface. However, as mentioned earlier (Section 5.1), low S/Fe ratios in the Copper Liquor Dam/Acid River waters (~1.5) could be due to low pH leaching of hematite/jarosite or residual felsic volcanic gangue material (Taylor and Whelan, 1942) rather than non-stoichiometric pyrite leaching or degassing of SO_2. It would be useful to examine the pyrite surfaces in the waste for evidence of elemental sulphur to help resolve which mechanism results in the low dissolved S/Fe ratios.

Interestingly, Brunner et al. (2008) and Yu et al. (2001) showed that during the initial stage (<400 h) of biotic pyrite oxidation experiments at pH 1.9–2.1, *A. ferrooxidans* leached pyrite non-stoichiometrically (S/Fe = 1.1), with ferrous iron as the dominant iron species, producing sulphate with $\delta^{18}O_{(SO4-H2O)} \approx 10‰$, a similar oxygen isotope signature to the Copper Liquor Dam/Acid River waters. A critical difference between the field data from the Copper Liquor Dam/Acid River and the Brunner et al. (2008)/Yu et al. (2001) experiments is that the initial stage experimental leaching was slow and produced low concentrations of dissolved products whereas the field data is indicative of high degrees of pyrite oxidation (605–1210 mM SO_4). Brunner et al. (2008) suggested that limited ferrous iron concentrations during initial stage leaching promoted a microbial metabolic strategy of S^0 oxidation rather than Fe^{2+} oxidation. In contrast, the Copper Liquor Dam/Acid River waters contain abundant Fe^{2+} (303–757 mM). Furthermore, microbiological data from similarly low pH, predominantly ferrous iron waters at Iron Mountain (Druschel et al., 2004 and references therein) show communities dominated by Fe-oxidizers and show that *A. ferrooxidans* is not a significant member of these communities at the low pHs relevant to the Copper Liquor Dam/Acid River waters. However, the current lack of microbiological data for Copper Liquor Dam/Acid River and uncertainties in metabolic pathways and their associated oxygen isotope fractionation means that the role of microbial oxidation of reduced sulphur compounds cannot be determined perfectly for these waters.

5.2.3. Tunnel inputs

Fig. 3 presents the pH, Zn/Cu molar ratios and isotope data for Tunnel 11 and Tunnel 16. These drainage waters emerge from underground workings and the drainage sources are therefore not as well constrained as Red River and Copper Liquor Dam/Acid River. The interesting aspect of this site is the shift in geochemistry and sulphate–oxygen isotopes of Tunnel 16 that occurs after January 2003, suggesting a change in the source of mine drainage and/or the mechanism of pyrite oxidation, perhaps to a similar source/mechanism as Tunnel 11 (Fig. 3). Based on the experimental results of Taylor et al. (1984b), the decrease in $\delta^{18}O_{(SO4-H2O)}$ may represent the transition from wet/dry to submersed conditions as groundwater levels rose again following the cessation of mining activities.

Low pH (e.g. 0.5–0.9, Druschel et al., 2004) waters with high $\delta^{18}O_{(SO4-H2O)}$ values (~13‰, Taylor and Wheeler, 1994) have also been sampled from tunnels draining the Richmond and Lawson mine tunnels at Iron Mountain. Variations in the chemistry and sulphate–oxygen isotope compositions sampled downstream of these sites have been attributed to (seasonal) wet/dry cycles (Taylor and Wheeler, 1994; Alpers et al., 2003; Druschel et al., 2004). Taylor and Wheeler (1994) interpreted high $\delta^{18}O_{(SO4-H2O)}$ values as due to the dissolution of secondary iron sulphate minerals formed from evaporating waters (with high $\delta^{18}O_{H2O}$) and/or formed from concentrated seeps of acid mine drainage at extremely low pH (Nordstrom et al., 2000) and elevated temperature (leading to partial oxygen equilibrium between sulphate and water). Unfortunately, no data exist on the underground source of Tunnel 16 drainage. It is possible that similar environments to Iron Mountain exist and that the high $\delta^{18}O_{(SO4-H2O)}$ values sampled in January 2003 were due to the dissolution of iron sulphate minerals by more dilute infiltrating waters.

Mass balance calculations for Tunnel 16 (see Section 5.1) show that 93–96% of dissolved S was derived from pyrite oxidation and that the Tunnel 16 (January 2003) drainage can be explained by congruent sulphide dissolution without the need for additional sulphur sinks such as SO_2 or S^0 (Fig. 5) or the dissolution of iron sulphate minerals (with S/Fe <2). The sulphite–water oxygen exchange model of Seal (2003) together with the pyrite oxidation scheme of Rimstidt and Vaughan (2003) provide a simpler explanation for sulphate–oxygen isotopes, predicting that the sulphate in the low pH (1.1–1.4) waters sampled from Tunnel 16 in January 2003 ($\delta^{18}O_{(SO4-H2O)} = 11.9–13.6‰$) was predominantly released as sulphite, although the equations from Holt et al. (1981) suggest that the conditions in the inaccessible, underground oxidation environment of Tunnel 16 may have been oxygen-limited as the oxygen-unlimited end-member equation predicts values over 100% (96–108%). Reduced oxygen levels are a possibility in disused underground workings.

Overall, the oxygen isotope data for Tunnel 16 can be interpreted as a decrease after January 2003 in the amount of S being released from the pyrite surface as sulphite rather than sulphate. Although this interpretation is consistent with current low pH pyrite oxidation models and data on the magnitude of sulphite–water oxygen exchange, it is not clear what conditions at the pyrite surface promote the release of sulphite rather than sulphate.

5.3. Directions for future work

The sulphite–water oxygen exchange model provides the most consistent explanation of sulphate–oxygen isotope data in this study but problems still remain with the model. In this section we identify areas for future work that are needed to improve our understanding.

The model predicts a range of 75–100% water–oxygen in the resultant sulphate, yet biotic and abiotic experiments at pH 2.0–2.5 with varying initial $\delta^{18}O_{H2O}$ values have shown values as low as 55% (Gould et al., 1989; Qureshi, 1986 in van Stempvoort and Krouse, 1994). A potential explanation is that sulphite oxidation passes through a $SO_3{}^{*-}$ intermediate which reacts with O_2 to give $SO_5{}^{*-}$ (Zhang and Millero, 1994; Ermakov et al., 1997; Brandt and van Eldik, 1998). Incomplete sulphite–water oxygen exchange at higher pH may also result in less water–oxygen being incorporated into the final sulphate (Krouse et al., 1991). Uncertainties also exist over the relative kinetics of bisulphite–water oxygen exchange at low pH and bisulphite oxidation by Fe^{3+}, O_2 or OH*, leading to the possibility of incomplete oxygen exchange in a kinetically controlled system if the bisulphite half-life in solution is less than the equilibrium oxygen exchange reaction. Further experiments are therefore needed to explicitly determine the fraction of atmospheric oxygen incorporated into sulphate from sulphite oxidation and the isotopic signature produced by sulphite–water oxygen exchange at low pH followed by oxidation to sulphate by Fe^{3+} or O_2. Information on the resultant sulphate isotopomers could be gained using the FTIR approach of Reedy et al. (1991, 1994).

Few studies have explicitly determined the percentage of water–oxygen incorporated into sulphate during pyrite oxidation (Balci et al., 2007; Gould et al., 1989; Qureshi, 1986 in van Stempvoort and Krouse, 1994). These studies span a range of conditions (aerobic/anaerobic, biotic/abiotic, pH 2.0–3.0) and incorporated 55 to ~100% water–oxygen. However, Fig. 7c shows that the $\delta^{18}O_{(SO4-H2O)}$ values for these experiments in the range of the Río Tinto data were below those of the Copper Liquor Dam/Acid River and Tunnel 16 (January 2003). Additional experiments of this type conducted under similar pH and redox conditions to the Río Tinto samples may help to constrain mechanisms further, as the stoichiometric and general isotope balance models predict much lower incorporation of water–oxygen than the sulphite–water exchange model.

Finally, Schippers et al. (1996) and Schippers et al. (1999) detected reduced sulphur compounds (mainly S^0 with minor $S_4O_6^{2-}$ and $S_5O_6^{2-}$) in experiments at pH 0.7–2.5, suggesting that more complicated

oxidation pathways may occur at low pH. They performed pyrite oxidation assays at pH 1.7 (i.e. the same pH as Red River) with Fe^{3+} and in the presence and absence of $AgNO_3$. The theory was that if thiosulphate was the first intermediate released into solution, it would rapidly form a $Ag_2S_2O_3$ precipitate which would decompose to the black, insoluble compound Ag_2S in acidic conditions. Note that Ag_2SO_3 is also insoluble, so thiosulphate release may not be distinguishable from sulphite release with this method. If it is assumed that only water–oxygen interacts with the surface-bound pyrite moiety and that any dissolved reduced sulphur compund (be it thiosulphate or sulphite) is oxidized to sulphate via a sulphite intermediate, then the direct release sulphate in the assay with Ag ions should have a $\delta^{18}O_{SO4}$ close to water whereas the dissolved sulphate in the assay without Ag ions should have a higher $\delta^{18}O_{SO4}$ due to sulphite–water oxygen exchange. These simple assays could help constrain hypotheses concerning the importance of sulphite–water oxygen exchange in modifying isotopic compositions, the importance of sulphoxyanion release at low pH and whether or not dissolved O_2 interacts directly with the surface-bound S-moiety.

6. Conclusions

Mass balance calculations predict that pyrite oxidation accounts for over 93% of the dissolved sulphate derived from sulphide oxidation in the low pH acid mine drainage inputs into the Río Tinto. Comparisons of the aqueous geochemistry emerging from underground tunnels with initial sulphide ore compositions show preferential oxidation of chalcopyrite and sphalerite, likely via a galvanic protection mechanism. Geochemical modelling predicts that dissolved Pb concentrations are limited by equilibrium with anglesite below pH 1.5 and coprecipitation with a jarosite phase above this pH.

Oxygen isotope data show a range of $\delta^{18}O_{(SO4-H2O)}$ values from 3.9 to 13.6‰, suggesting that different oxidation pathways occur at different sites within the catchment. The Río Tinto data can be most consistently interpreted using the sulphite–water oxygen exchange model, assuming that sulphate is either released directly to solution or that it is oxidized via a dissolved sulphite intermediate that exchanges oxygen rapidly with water. However, this model needs to be expanded to account for different routes of sulphite oxidation, to explain experimental pyrite oxidation data that shows >25% atmospheric oxygen in sulphate and to properly evaluate the magnitude of sulphite–water oxygen fractionation at low pH. Recommendations for future work have therefore been proposed in this paper to further our understanding of oxygen isotopes in acid mine drainage.

Acknowledgements

Chris Hubbard would like to thank the University of Reading for a Postgraduate Research Studentship. The isotopic analyses described in this paper were performed at the Jet Propulsion Laboratory (JPL), California Institute of Technology, under a contract with the National Aeronautics and Space Administration (NASA) with support from JPL's Research and Technology Development Program via a grant to MC. Particular thanks are due to Randall Mielke for assistance with the isotopic analyses. We thank the Fundación Río Tinto and especially Maite López for their help and for permission to access the Mine area and take samples. Finally, we would like to thank Greg Druschel and an anonymous reviewer for their helpful comments and suggestions and David Rickard for his editorial role.

References

Aguilera, A., Souza-Egipsy, V., Gómez, F., Amils, R., 2007a. Development and structure of eukaryotic biofilms in an extreme acidic environment, Río Tinto SW, Spain. Microb. Ecol. 53, 294–305.

Aguilera, A., Zettler, E., Gómez, F., Amaral-Zettler, L., Rodríguez, N., Amils, R., 2007b. Distribution and seasonal variability in the benthic eukaryotic community of Río Tinto SW, Spain, an acidic, high metal extreme environment. Syst. Appl. Microbiol. 30, 531–546.

Alpers, C.N., Nordstrom, D.K., Spitzley, J., 2003. Extreme acid mine drainage from a pyritic massive sulfide deposit: the Iron Mountain end-member. In: Jambor, J.L., Blowes, D.W., Ritchie, A.I.M. (Eds.), Environmental Aspects of Mine Wastes. Mineralogical Association of Canada.

Amils, R., González-Toril, E., Fernández-Remolar, D., Gómez, F., Aguilera, A., Rodríguez, N., Malki, M., García-Moyano, A., Fairén, A.G., de la Fuente, V., Sanz, J.L., 2007. Extreme environments as Mars terrestrial analogs: the Rio Tinto case. Planet. Space Sci. 55, 370–381.

Avery, D., 1974. Not on Queen Victoria's Birthday: the Story of the Rio Tinto Mines. Collins, London.

Balci, N., Shanks III, W.C., Mayer, B., Mandernack, K.W., 2007. Oxygen and sulfur isotope systematics of sulfate produced by bacterial and abiotic oxidation of pyrite. Geochim. Cosmochim. Acta 71, 3796–3811.

Ball, J.W., Nordstrom, D.K., 1991. User's manual for WATEQ4F, with revised thermodynamic data base and test cases for calculating speciation of major, trace, and redox elements in natural waters. USGS Open-File Report, pp. 91–183.

Bao, H., 2006. Purifying barite for oxygen isotope measurement by dissolution and reprecipitation in a chelating solution. Anal. Chem. 78, 304–309.

Basolo, F., Pearson, R.G., 1967. Mechanisms of inorganic reactions — a study of metal complexes in solution. John Wiley and Sons, New York.

Betts, R.H., Voss, R.H., 1970. Kinetics of oxygen exchange between sulfite ion and water. Can. J. Chem. 48, 2035–2041.

Borda, M.J., Elsetinow, A.R., Strongin, D.R., Schoonen, M.A., 2003a. A mechanism for the production of hydroxyl radical at surface defect sites on pyrite. Geochim. Cosmochim. Acta 67, 935–939.

Borda, M.J., Strongin, D.R., Schoonen, M.A., 2003b. A vibrational spectroscopic study of the oxidation of pyrite by ferric iron. Am. Mineral. 88, 1318–1323.

Bottrell, S.H., 2007. Stable isotopes in aqueous sulphate as tracers of natural and contaminant sulphate sources: a reconnaissance study of the Xingwen karst aquifer, Sichuan, China. In: Parise, M., Gunn, J. (Eds.), Natural and Anthropogenic Hazards in Karst Areas: Recognition, Analysis and Mitigation. Geological Society, London, Special Publications, vol. 279, pp. 123–135.

Brandt, C., van Eldik, R., 1998. Kinetics and mechanism of the ironIII-catalyzed autoxidation of sulfurIV oxides in aqueous solution. The influence of pH, medium and aging. Transition Met. Chem. 23, 667–675.

Braungardt, C.B., Achterberg, E.P., Elbaz-Poulichet, F., Morley, N.H., 2003. Metal geochemistry in a mine-polluted estuarine system in Spain. Appl. Geochem. 18, 1757–1771.

Brown, E., Skougstad, M.W., Fishman, M.J., 1970. Methods for Collection and Analysis of Water Samples for Dissolved Minerals and Gases: Techniques of Water-Resources Investigations of the U.S. Geological Survey. U.S. Government Printing Office, Washington, DC.

Brunner, B., Mielke, R.E., Coleman, M., 2006. Abiotic oxygen isotope equilibrium fractionation between sulfite and water. American Geophysical Union, Fall Meeting 2006, abstract #V11C-0601.

Brunner, B., Yu, J.-Y., Mielke, R.E., MacAskill, J.A., Madzunkov, S., McGenity, T.J., Coleman, M., 2008. Different isotope and chemical patterns of pyrite oxidation related to lag and exponential growth phases of *Acidithiobacillus ferrooxidans* reveal a microbial growth strategy. Earth Planet. Sci. Lett. 270, 63–72.

Buckby T. 2003. Processes of persistent metal contamination in the Río Tinto, South West Spain. Ph.D. thesis, Reading Univ.

Buckby, T., Black, S., Coleman, M.L., Hodson, M.E., 2003. Fe-sulfate-rich evaporative mineral precipitates from the Rio Tinto, southwest Spain. Mineral. Mag. 67, 263–278.

Butler, T.W., 2007. Isotope geochemistry of drainage from an acid mine impaired watershed, Oakland, California,. Appl. Geochem. 22, 416–1426.

Cánovas, C.R., Olias, M., Nieto, J.M., Sarmiento, A.M., Cerón, J.C., 2007. Hydrogeochemical characteristics of the Odiel and Tinto rivers SW Spain. Factors controlling metal contents. Sci. Total Environ. 373, 363–382.

Cánovas, C.R., Hubbard, C.G., Olias, M., Nieto, J.M., Black, S., Coleman, M.L., 2008. Hydrochemical variations and contaminant load in the Río Tinto Spain during flood events. J. Hydrol. 350, 25–40.

Celle-Jeanton, H., Travi, Y., Blavoux, B., 2001. Isotopic typology of the precipitation in the Western mediterranean region at three different time scales. Geophys. Res. Lett. 28, 1215–1218.

Chapman, B.M., Jones, D.R., Jung, R.F., 1983. Processes controlling metal–ion attenuation in acid-mine drainage streams. Geochim. Cosmochim. Acta 47, 1957–1973.

Chiba, H., Saki, H., 1985. Oxygen isotope exchange rate between dissolved sulfate and water at hydrothermal temperatures. Geochim. Cosmochim. Acta 49, 993–1000.

Cortecci, G., Dinelli, E., Boschetti, T., Arbizzani, P., Pompilio, L., Mussi, M., 2008. The Serchio River catchment, northern Tuscany: geochemistry of stream waters and sediments, and isotopic composition of dissolved sulfate. Appl. Geochem. 23, 1513–1543.

Descostes, M., Vitorge, P., Beaucaire, C., 2004. Pyrite dissolution in acidic media. Geochim. Cosmochim. Acta 68, 4559–4569.

Druschel, G., Borda, M., 2006. Comment on "Pyrite dissolution in acidic media" by M. Descostes, P. Vitorge, and C. Beaucaire. Geochim. Cosmochim. Acta 70, 5246–5250.

Druschel, G.K., Hamers, R.J., Banfield, J.F., 2003a. Kinetics and mechanism of polythionate oxidation to sulfate at low pH by O_2 and Fe^{3+}. Geochim. Cosmochim. Acta 67, 4457–4469.

Druschel, G.K., Hamers, R.J., Luther, G.W.I., Banfield, J.F., 2003b. Kinetics and mechanism of trithionate and tetrathionate oxidation at low pH by hydroxyl radicals. Aquat. Geochem. 9, 145–164.

Druschel, G.K., Baker, B.J., Gihring, T.M., Banfield, J.F., 2004. Acid mine drainage biogeochemistry at Iron Mountain, California. Geochem. Trans. 5 (2), 13–32.

Elbaz-Poulichet, F., Braungardt, C., Achterberg, E., Morley, N., Cossa, D., Beckers, J.-M., Nomérange, P., Cruzado, A., Leblanc, M., 2001. Metal biogeochemistry in the Tinto–

Odiel rivers Southern Spain and in the Gulf of Cadiz: a synthesis of the results of TOROS project. Cont. Shelf Res. 21, 1961–1973.
Ermakov, A.N., Poskrebyshev, G.A., Purmal, A.P., 1997. Sulfite oxidation: the state-of-the-art of the problem. Kinet. Catal. 38, 295–308.
Epstein, S., Mayeda, T., 1953. Variation of O-18 content of waters from natural sources. Geochim. Cosmochim. Acta 4, 213–224.
Fernández-Remolar, D.C., Morris, R.V., Gruener, J.E., Amils, R., Knoll, A.H., 2005. The Rio Tinto basin, Spain: mineralogy, sedimentary geobiology, and implications for interpretation of outcrop rocks at Meridiani Planum, Mars. Earth Planet. Sci. Lett. 240, 149–167.
Fuge, R., Pearce, F.M., Pearce, N.G., Perkins, W.T., 1993. Geochemistry of Cd in the secondary environment near abandoned metalliferous mines, Wales. Appl. Geochem. Suppl. Iss. 2, 29–35.
Gammons, C.H., Nimick, D.A., Parker, S.R., Snyder, D.M., McCleskey, R.B., Amils, R., Poulson, S.R., 2008. Photoreduction fuels biogeochemical cycling of iron in Spain's acid rivers. Chem. Geol. 252, 202–213.
Goldhaber, M.B., 1983. Experimental study of metastable sulfur oxyanion formation during pyrite oxidation at pH 6–9 and 30 °C. Am. J. Sci. 283, 193–217.
Gonzalez-Toril, E., Gomez, F., Rodriguez, N., Fernandez-Remolar, D., Zuluaga, J., Marin, I., Amils, R., 2003a. Geomicrobiology of the Tinto River, a model of interest for biohydrometallurgy. Hydrometallurgy 71, 301–309.
Gonzalez-Toril, E., Llobet-Brossa, E., E.O., C., Amann, R., Amils, R., 2003b. Microbial ecology of an extreme acidic environment, the Tinto River. Appl. Environ. Microbiol. 69, 4853–4865.
Gould, W.D., McCready, R.G.L., Rajan, S., Krouse, H.R., 1989. Stable isotope composition of sulfate produced during bacterial oxidation of various metal sulfides. In: Salley, J., McCready, R.G.L., Wichlacz, P.L. (Eds.), Biohydrometallurgy 1989, CANMET SP89-10, pp. 81–92.
Hamer, W.J., Wu, Y.-C., 1972. J. Phys. Chem. Ref. Data 1, 1047.
Hamlin, S.N., Alpers, C.N., 1995. Hydrogeology and geochemistry of acid mine drainage in ground water in the vicinity of Penn Mine and Camanche Reservoir, Calaveras County, California: first-year summary. USGS Water Resources Investigating Report 94-4040.
Hamlin, S.N., Alpers, C.N., 1996. Hydrogeology and geochemistry of acid mine drainage in ground water in the vicinity of Penn Mine and Camanche Reservoir, Calaveras County, California: second-year summary, 1992–93. USGS Water Resources Investigating Report 96-4257.
Haubrich, F., Tichomirowa, M., 2002. Sulfur and oxygen isotope geochemistry of acid mine drainage — the polymetallic sulfide deposit “Himmelfahrt Fundgrube” in Freiberg Germany. Isot. Environ. Health Stud. 38, 121–138.
Hochella, M.F., Moore, J.N., Golla, U., Putnis, A., 1999. A TEM study of samples from acid mine drainage systems: metal–mineral association with implications for transport. Geochim. Cosmochim. Acta 63, 3395–3406.
Hoering, T.C., Kennedy, J.W., 1957. The exchange of oxygen between sulfuric acid and water. J. Am. Chem. Soc. 79, 56–60.
Holt, B.D., Kumar, R., Cunningham, P.T., 1981. Oxygen-18 study of the aqueous-phase oxidation of sulfur dioxide. Atmos. Environ. 15, 557–566.
Huie, R.E., Neta, P., 1987. Rate constants for some oxidations of SIV by radicals in aqueous-solutions. Atmos. Environ. 21, 1743–1747.
Hudson-Edwards, K.A., Schell, C., Macklin, M.G., 1999. Mineralogy and geochemistry of alluvium contaminated by metal mining in the Rio Tinto area, southwest Spain. Appl. Geochem. 14, 1015–1030.
Jambor, J.L., Nordstrom, D.K., Alpers, C.N., 2000. Metal-sulfate salts from sulfide mineral oxidation. In: Alpers, C.N., Jambor, J.L., Nordstrom, D.K. (Eds.), Sulfate Minerals — Crystallography, Geochemistry and Environmental Significance. Reviews in Mineralogy and Geochemistry, vol. 40. Mineralogical Society of America, Washington D.C.
Kelly, D.P., 1999. Thermodynamic aspects of energy conservation by chemolithotrophic sulfur bacteria in relation to the sulfur oxidation pathways. Arch. Microbiol. 171, 219–229.
Knoller, K., Fauville, A., Mayer, B., Strauch, G., Friese, K., Veizer, J., 2004. Sulfur cycling in an acid mining lake and its vicinity in Lusatia, Germany. Chem. Geol. 204, 303–323.
Kolthoff, J.M., Meehan, E.J., Sandell, E.B., Bruckenstein, S., 1969. Quantitative Chemical Analysis, 4th Ed. MacMillan, New York. USA.
Kroopnick, P., Craig, H., 1972. Atmospheric oxygen: isotopic composition and solubility fractionation. Science 175, 54–55.
Krouse, H.R., Gould, W.D., McCready, R.G.L., Rajan, S., 1991. O-18 incorporation into sulfate during the bacterial oxidation of sulfide minerals and the potential for oxygen isotope exchange between O_2, H_2O and oxidized sulfur intermediates. Earth Planet. Sci. Lett. 107, 90–94.
Kwong, Y.T.J., Swerhone, G.W., Lawrence, J.R., 2003. Galvanic sulphide oxidation as a metal-leaching mechanism and its environmental implications. Geochem. Expl. Env. Anal. 3, 337–344.
Leblanc, M., Morales, J.A., Borrego, J., Elbaz-Poulichet, F., 2000. 4,500 year-old mining pollution in southwestern Spain: long-term implications for modern mining pollution. Econ. Geol. 95, 655–662.
Lefticariu, L., Schimmelmann, A., Pratt, L.M., Ripley, E.M., 2007. Oxygen isotope partitioning during oxidation of pyrite by H_2O_2 and its dependence on temperature. Geochim. Cosmochim. Acta 71, 5072–5088.
López-Archilla, A.I., Marin, I., Amils, R., 2001. Microbial community composition and ecology of an acidic aquatic environment: the Tinto River, Spain. Microb. Ecol. 41, 20–35.
López-Archilla, A.I., Gerard, E., Moreira, D., Lopez-Garcia, P., 2004. Macrofilamentous microbial communities in the metal-rich and acidic River Tinto, Spain. FEMS Microbiol. Lett. 235, 221–228.
Lowson, R.T., 1982. Aqueous pyrite oxidation by molecular oxygen. Chem. Rev. 82, 461–491.
Luther III, G.W., 1987. Pyrite oxidation and reduction: molecular orbital theory considerations. Geochim. Cosmochim. Acta 51, 3193–3199.
Luther III, G.W., 1997. Comment on "Confirmation of a sulfur-rich layer on pyrite after oxidative dissolution by Fe(III) ions around pH 2" by K. Sasaki, M. Tsunekawa, T. Ohtsuka, and H. Konno. Geochim. Cosmochim. Acta 61, 3269–3271.
McGuire, M.M., Edwards, K.J., Banfield, J.F., Hamers, R.J., 2001. Kinetics, surface chemistry, and structural evolution of microbially mediated sulfide mineral dissolution. Geochim. Cosmochim. Acta 65, 1243–1258.
Migaszewski, Z.M., Galuszka, A., Halas, S., Dołęgowska, S., Dąbek, J., Starnawska, E., 2008. Geochemistry and stable sulfur and oxygen isotope ratios of the Podwiśniówska pit pond water generated by acid mine drainage (Holy Cross Mountains, south-central Poland). Appl. Geochem. 23, 3620–3634.
Millero, F.J., 2001. The Physical Chemistry of Natural Waters. John Wiley and Sons Inc., New York.
Moses, C.O., Nordstrom, D.K., Herman, J.S., Mills, A.L., 1987. Aqueous pyrite oxidation by dissolved oxygen and by ferric iron. Geochim. Cosmochim. Acta 51, 1561–1571.
Nehlig, P., Cassard, D., Marcoux, E., 1998. Geometry and genesis of feeder zones of massive sulfide deposits: constraints from the Rio Tinto ore deposit Spain. Miner. Depoita. 33, 137–149.
Nesbitt, H.W., Muir, I.J., 1994. X-ray photoelectron spectroscopic study of a pristine pyrite surface reacted with water-vapor and air. Geochim Cosmochim. Acta 58, 4667–4679.
Nordstrom, D.K., Wilde, F.D., 1998. Reduction–oxidation potential electrode method. National Field Manual for the Collection of Water Quality Data, U.S. Geological Survey Techniques of Water-Resources Investigations, Book 9; Chapter 6.5.
Nordstrom, D.K., Alpers, C.N., 1999. Geochemistry of Acid Mine Waters. In: Plumlee, G.D., Logsdon, M.J. (Eds.), The Environmental Geochemistry of Mineral Deposits. Part A: Processes, Techniques, and Health Issues. Society of Economic Geologists.
Nordstrom, D.K., Alpers, C.N., Ptacek, C.J., Blowes, D., 2000. Negative pH and extremely acidic mine waters from Iron Mountain, California. Environ. Sci. Technol. 34, 254–258.
Nordstrom, D.K., Wright, W.G., Mast, M.A., Bove, D.J., Rye, R.O., 2007. Aqueous-sulfate stable isotopes — a study of mining-affected and undisturbed acidic drainage. Chapter E8 In USGS Professional Paper, p. 1651.
Olias, M., Canovas, C.R., Nieto, J.M., Sarmiento, A.M., 2006. Evaluation of the dissolved contaminant load transported by the Tinto and Odiel rivers South West Spain. Appl. Geochem. 21, 1733–1749.
Parkhurst, D.L., Appelo, C.A.J., 1999. User's guide to PHREEQC version 2 — a computer program for speciation, batch-reaction, one-dimensional transport, and inverse geochemical calculations. USGS Water Resources Investigations Report, pp. 99–4259.
Parro, V., Rodriguez-Manfredi, J.A., Briones, C., Compostizo, C., Herrero, P.L., Vez, E., Sebastian, E., Moreno-Paz, M., Garcia-Villadangos, M., Fernandez-Calvo, P., Gonzalez-Toril, E., Perez-Mercader, J., Fernandez-Remolar, D., Gomez-Elvira, J., 2005. Instrument development to search for biomarkers on Mars: terrestrial acidophile, iron-powered chemolithoautotrophic communities as model systems. Planet. Space Sci. 53, 729–737.
Pellicori, D.A., Gammons, C.H., Poulson, S.R., 2005. Geochemistry and stable isotope composition of the Berkeley pit lake and surrounding mine waters, Butte, Montana. Appl. Geochem. 20, 2116–2137.
Qureshi R.M. 1986. The isotopic composition of aqueous sulfate a laboratory investigation. Ph.D. thesis, Waterloo Univ.
Reedy, B.J., Beattie, J.K., Lowson, R.T., 1991. A vibrational spectroscopic O-18 tracer study of pyrite oxidation. Geochim. Cosmochim. Acta 55, 1609–1614.
Reedy, B.J., Beattie, J.K., Lowson, R.T., 1994. O-18 sulfate isotopomers monitored by infrared-spectroscopy. Appl. Spectrosc. 48, 691–694.
Rimstidt, J., Vaughan, D., 2003. Pyrite oxidation: a state-of-the-art assessment of the reaction mechanism. Geochim. Cosmochim. Acta 67, 873–880.
Romero, A., Gonzalez, I., Galan, E., 2006. Estimation of potential pollution of waste mining dumps at Pena del Hierro Pyrite Belt, SW Spain as a base for future mitigation actions. Appl. Geochem. 21, 1093–1108.
Rosso, K.M., Becker, U., Hochella, M.F., 1999. The interaction of pyrite {100} surfaces with O_2 and H_2O: fundamental oxidation mechanisms. Am. Mineral. 84, 1549–1561.
Ruiz, F., González-Regalado, M.L., Borrego, J., Morales, J.A., Pendón, J.G., Muñoz, J.M., 1998. Stratigraphic sequence, elemental concentrations and heavy metal pollution in Holocene sediments from the Tinto-Odiel Estuary, southwestern Spain. Environ. Geol. 34, 270–278.
Salkield, L.U., 1987. A Technical History of the Rio Tinto Mines: Some Notes on Exploitation from pre-Phoenician Times to the 1950s. The Institute of Mining and Metallurgy, London.
Sánchez España, J., López Pamo, E., Santofimia, E., Aduvire, O., Reyes, J., Barettino, D., 2005. Acid mine drainage in the Iberian Pyrite Belt (Odiel river watershed, Huelva, SW Spain): geochemistry, mineralogy and environmental implications. Appl. Geochem. 20, 1320–1356.
Sasaki, K., Tsunekawa, M., Ohtsuka, T., Konno, H., 1995. Confirmation of a sulfur-rich layer on pyrite after oxidative dissolution by FeIII ions around pH 2. Geochim. Cosmochim. Acta 59, 3155–3158.
Schippers, A., Jozsa, P.G., Sand, W., 1996. Sulfur chemistry in bacterial leaching of pyrite. Appl. Environ. Microbiol. 62, 3424–3431.
Schippers, A., Rohwerder, T., Sand, W., 1999. Intermediary sulfur compounds in pyrite oxidation: implications for bioleaching and biodepyritization of coal. Appl. Microbiol. Biotechnol. 52, 104–110.
Seal II, R.R., 2003. Stable-isotope geochemistry of mine waters and related solids. In: Jambor, J.L., Blowes, D.W., Ritchie, A.I.M. (Eds.), Environmental Aspects of Mine Wastes. Mineralogical Association of Canada.
Seal II, R.R., Hammarstrom, J.M., Southworth, C.S., Meier, A.L., Haffner, D.P., Schultz, A.P., Plumlee, G.S., Flohr, M.J.K., Jackson, J.C., Smith, S.M., Hageman, P.L., 1998. Preliminary report on water quality associated with the abandoned Fontana and

Hazel Creek mines, Great Smoky Mountains National Park, North Carolina and Tennessee. YSGS Open-File Report, pp. 98–476.
Seal II, R.R., Hammarstrom, J.M., Johnson, A.N., Piatak, N.M., Wandless, G.A., 2008. Environmental geochemistry of a Kuroko-type massive sulfide deposit at the abandoned Valzinco mine, Virginia, USA. Appl. Geochem. 23, 320–342.
Smuda, J., Dold, B., Spangenberg, J.E., Pfeifer, H.-R., 2008. Geochemistry and stable isotope composition of fresh alkaline porphyry copper tailings: Implications on sources and mobility of elements during transport and early stages of deposition. Chem. Geol. 256, 62–76.
Spangenberg, J., Dold, B., Vogt, M.-L., Pfeifer, H.R., 2007. The stable hydrogen and oxygen isotope composition of waters from mine tailings in different climatic environments. Environ. Sci. Tech. 41, 1870–1876.
Sracek, O., Choquette, M., Gélinas, P., Lefebvre, R., Nicholson, R.V., 2004. geochemical characterization of acid mine drainage from a waste rock pile, Mine Doyon, Québec, Canada. J. Cont. Hydrol. 69, 45–71.
Suzuki, I., Chan, C.W., Takeuchi, T.L., 1994. Oxidation of inorganic sulfur-compounds by *Thiobacilli*. In: Alpers, C.N., Blowes, D.W. (Eds.), Environmental Geochemistry of Sulfide Oxidation. American Chemical Society.
Taylor, J.H., Whelan, P.F., 1942. The leaching of cupreous pyrites and the precipitation of copper at Rio Tinto, Spain. Trans. Inst. Min. Metall. 52, 35–96.
Taylor, B.E., Wheeler, M.C., 1994. Sulfur- and oxygen-isotope geochemistry of acid mine drainage in the western United States. In: Alpers, C.N., Blowes, D.W. (Eds.), Environmental Geochemistry of Sulfide Oxidation. American Chemical Society.
Taylor, B.E., Wheeler, M.C., Nordstrom, D.K., 1984a. Isotope composition of sulfate in acid-mine drainage as measure of bacterial oxidation. Nature 308, 538–541.
Taylor, B.E., Wheeler, M.C., Nordstrom, D.K., 1984b. Stable isotope geochemistry of acid-mine drainage — experimental oxidation of pyrite. Geochim. Cosmochim. Acta 48, 2669–2678.
Tornos, F., 2006. Environment of formation and styles of volcanogenic massive sulfides: the Iberian Pyrite Belt. Ore Geol. Rev. 28, 259–307.
van Everdingen, R.O., Krouse, H.R., 1985. Isotope composition of sulfates generated by bacterial and abiological oxidation. Nature 315, 395–396.
van Geen, A., Adkins, J.F., Boyle, E.A., Nelson, C.H., Palanques, A., 1997. A 120 yr record of widespread contamination from mining of the Iberian pyrite belt. Geology 25, 291–294.
van Stempvoort, D.R., Krouse, H.R., 1994. Controls of $\delta^{18}O$ in sulfate. In: Alpers, C.N., Blowes, D.W. (Eds.), Environmental Geochemistry of Sulfide Oxidation. American Chemical Society.
Vogel A.I. and Jeffery G.H. 1989. Textbook of quantitative chemical analysis, 5th edition Longman Scientific & Technical. Wiley, Harlow, Essex, England. 877 p.
Yu, J.Y., McGenity, T.J., Coleman, M.L., 2001. Solution chemistry during the lag phase and exponential phase of pyrite oxidation by *Thiobacillus ferrooxidans*. Chem. Geol. 175, 307–317.
Zettler, L.A.A., Gomez, F., Zettler, E., Keenan, B.G., Amils, R., Sogin, M.L., 2002. Eukaryotic diversity in Spain's River of Fire — this ancient and hostile ecosystem hosts a surprising variety of microbial organisms. Nature 417, 137–137.
Zhang, J.-Z., Millero, F.J., 1994. Kinetics of oxidation of hydrogen sulfide in natural waters. In: Alpers, C.N., Blowes, D.W. (Eds.), Environmental Geochemistry of Sulfide Oxidation. American Chemical Society.